Stress and Lifetime Calculations for First Wall and Blanket Structural Components

Part I:
Crack Propagation in Tubes

T. Fett, D. Munz
Institut für Reaktorbauelemente
(Zuverlässigkeit und Schadenskunde im Maschinenbau)
Projekt Kernfusion

Kernforschungszentrum Karlsruhe

KERNFORSCHUNGSZENTRUM KARLSRUHE

Institut für Reaktorbauelemente

(Zuverlässigkeit u. Schadenskunde im Maschinenbau)

Projekt Kernfusion

KfK 3875

STRESS AND LIFETIME CALCULATIONS FOR FIRST
WALL AND BLANKET STRUCTURAL COMPONENTS

Part I: Crack propagation in tubes

T. Fett, D. Munz

Kernforschungszentrum Karlsruhe GmbH, Karlsruhe

Stress and lifetime calculations for first wall and blanket components
Part I: Crack propagation in tubes

In this report the lifetime of first wall and blanket structures of fusion reactors is investigated. The extension of small pre-existing cracks by the cyclic operation of a fusion reactor seems to be the most important failure mode. The special application of the present investigation are tubes acting directly as parts of the first wall and affected by various radiation effects. The outer surface is asymmetrically heated and by combination of thermal extension, swelling, irradiation creep and internal pressure a complex time dependent stress distribution results. Crack growth until failure caused by cyclic operation of the reactor is computed by application of fracture mechanical methods.

Spannungs- und Lebensdauerberechnungen für erste Wand- und Blanket-Komponenten
Teil I: Rißwachstum in Rohren

Dieser Bericht befaßt sich mit der Lebensdauer der ersten Wand und mit Blankets von Fusionsreaktoren. Die Ausbreitung kleiner vorhandener Risse durch die zyklische Belastung aufgrund des pulsierenden Reaktorbetriebs scheint die wesentlichste Versagensursache zu sein. Als spezieller Anwendungsfall dieses Teils der Untersuchung wurden Rohre betrachtet, die direkt der Plasmastrahlung und somit unterschiedlichen Bestrahlungseinflüssen ausgesetzt sind. Durch die unsymmetrische Oberflächenheizung resultieren aufgrund der thermischen Ausdehnung, des Schwellens, strahlungsinduzierten Kriechens und des Innendrucks komplexe zeitabhängige Spannungsverteilungen. Das durch die zyklische Arbeitsweise des Reaktors bedingte Rißwachstum wird mit bruchmechanischen Methoden bis zum Versagen berechnet.

Table of Contents

1. Introduction

The lifetime of the first wall and blanket system of fusion reactors can be limited by different failure modes such as excessive plastic deformation due to creep, creep rupture, crack initiation and crack growth resulting from cyclic loading, wall erosion caused by sputtering, or by a combination of these effects. The extension of small cracks - generated in the welding process during fabrication - through cyclic operation of a fusion reactor seems to be the most important failure mode. In the past, lifetime calculations were performed, often with the help of constrained plates simulating the first wall [1 - 13]. As an alternative and a further step in the direction of more complex structures, the behaviour of pressurized tubes constrained by bending has been investigated.

The purpose of this investigation is to exhibit the general behaviour of first wall and blanket structures, and to obtain information about the different influencing factors. The calculations are a basis for further, more detailed considerations. A special application of the present investigation are tubes acting directly as parts of the first wall [14]. Such tubes are exposed for various radiation effects. The outer surface is heated by an asymmetrically distributed neutron irradiation. This gives rise to a volumetric heat component and void swelling. In the presence of mechanical stresses also irradiation creep will occur. Internal pressure leads to additive tensile stresses in the tube wall. In addition, sputtering of the surface due to bombardment by fast particles has to be taken into account. By combination of thermal extension, swelling, irradiation creep and internal pressure a complex time dependent stress distribution results restraining free deformation of the tube because of geometrical boundary conditions. In most cases free bending is impossible.

Stainless steel SS 316 (20% CW) was chosen as the tube material because an extended data base is available for this material. Some of the material data used were taken from the investigation of Watson et al [5,6]; they will not be discussed here. In a further study a broader data basis and alternative materials will have to be considered.

The paper is organized in the following way:
- detailed calculation of temperature and stress distribution,
- distribution of neutrons,
- consideration of swelling and irradiation creep,
- time-dependent change of stresses due to creep and swelling,
- computation of stress intensity factors and crack growth due to cyclic operation.

2. Temperature and thermal stresses in tubes

2.1 Basic equations and boundary conditions

Whilst stationary temperature distributions in asymmetrically heated tubes are well-known from analysis [15], instationary distributions are often treated by numerical solution of the equation describing instationary heat conduction [16,17], in the last 10 years mainly by finite-element analysis [18,19]. In this paper an analytical solution of this problem will be given.

The basis of the following calculations is the equation for instationary heat conduction

$$\frac{\partial T}{\partial t} = \varkappa \, \Delta T \qquad ; \qquad \varkappa = (\Lambda \, c \, d)^{-1} \qquad (1)$$

where T is the temperature, t the time, $1/\Lambda$ the thermal conductivity, c the specific heat, and d the density.
The laplacian is written in cylindric coordinates as

$$\Delta = \frac{1}{\varrho} \frac{\partial}{\partial \varrho} + \frac{\partial^2}{\partial \varrho^2} + \frac{1}{\varrho^2} \frac{\partial^2}{\partial \varphi^2} \qquad (2)$$

The geometric units are shown in Fig. 1. The boundary conditions are given by a constant inner surface temperatur (arbitrarily chosen: T = 0) and the heat flux $\dot{Q}$ at the outer surface.

$$T(\varrho = r) = 0 \qquad (3)$$

$$\frac{\partial T}{\partial \varrho} (\varrho = R) = -\Lambda \, \dot{Q}(\varphi) \qquad (4)$$

2.1.1 Fourier components of the time-dependent temperature distribution

To solve Eq. (1) under boundary conditions given by Eqs. (3) and (4) it is usual to carry out a Laplace transformation to eliminate the time dependence.

If $\bar{T}$ denotes the Laplace transformation of the temperature T

$$\bar{T} = \int_0^\infty T(t) \exp(-pt) \, dt \tag{5}$$

one obtains from Eq. (1), considering the initial condition $T(t=0)=0$,

$$\frac{\partial^2 \bar{T}}{\partial \varrho^2} + \frac{\partial \bar{T}}{\varrho \, \partial \varrho} + \frac{\partial^2 \bar{T}}{\varrho^2 \, \partial \varphi^2} - q^2 \, \bar{T} = 0 \tag{6}$$

with $q^2 = p/\varkappa$.

Since Eq. (6) is dependent only on ϱ and φ, insertion of the usual set-up

$$\bar{T}(\varrho,\varphi) = f(\varrho) \cdot g(\varphi) \tag{7}$$

into Eq. (6) gives, after separation of both variables,

$$\frac{\varrho^2}{f} \frac{\partial^2 f}{\partial \varrho^2} + \frac{\varrho}{f} \frac{\partial f}{\partial \varrho} - \varrho^2 q^2 = \frac{-\partial^2 g}{g \, \partial \varphi^2} \tag{8}$$

As the left-hand side is not dependent on φ and the right-hand side does not depend on ϱ, both sides must be constants (γ^2). From the periodicity of the temperature distribution one can conclude that γ must be an integer value (n). So the φ-dependency is given by

$$g_n(\varphi) = a_n \cos n\varphi + b_n \sin n\varphi \tag{9}$$

From the left-hand side it results

$$\varrho^2 f'' + \varrho f' - (q^2 \varrho^2 + n^2) f = 0 \tag{10}$$

The solutions of this differential equation are the cylindrical functions

$$f_n = Z_n(q \cdot \varrho) \tag{11}$$

A system of solutions can be composed by modified Bessel functions of nth order

$$f_n = B_1 I_n(q \varrho) + B_2 K_n(q \varrho) \qquad\qquad B_1, B_2 = \text{constants} \tag{12}$$

So, the general solution can be written as

$$\bar{T}_n(\varrho, \varphi) = [A_n I_n(q \varrho) + B_n K_n(q \varrho)] \,(\cos n\varphi + C_n \sin n\varphi) \tag{13}$$

The ϱ dependent part of Eq. (13) is denoted $\bar{T}_{n\varrho}$

$$\bar{T}_{n\varrho} = A_n I_n(q \varrho) + B_n K_n(q \varrho) \tag{14}$$

The Laplace-transformed boundary conditions for $\cos \varphi$ -terms, i.e. the only terms of interest in this report, are

$$\bar{T}(\varrho = r) = 0 \tag{15}$$

$$\frac{\partial \bar{T}}{\partial \varrho}(\varrho = R) = \frac{D}{p} = \varkappa \frac{D}{q^2} \qquad\qquad D = -\Lambda \dot{Q} \tag{16}$$

If D_n denotes the nth Fourier component of D, the boundary conditions of the related temperature components become

$$\bar{T}_{n\varrho}(\varrho = r) = 0 \tag{17}$$

$$\frac{\partial \bar{T}_{n\varphi}}{\partial \varrho}(\varrho = R) = \frac{D_n}{p} \tag{18}$$

Substituting Eq. (14) into Eq. (17) yields

$$B_n = -A_n I_n(qr)/K_n(qr)$$ (19)

and thus instead of Eq. (14)

$$\bar{T}_n = \frac{A_n}{K_n(qr)}[I_n(q\varrho) K_n(qr) - I_n(qr) K_n(q\varrho)]$$ (20)

From the boundary condition (18) one obtains

$$\frac{\partial \bar{T}_{n\varrho}}{\partial \varrho}\bigg|_R = \frac{D_n}{p} = \frac{A_n q}{K_n(qr)}[I_n'(qR)K_n(qr) - I_n(qr)K_n'(qR)]$$ (21)

and by combination of Eqs. (14, 19, 21)

$$\bar{T}_{n\varrho} = \frac{D_n}{pq} \cdot \frac{I_n(q\varrho) K_n(qr) - I_n(qr) K_n(q\varrho)}{I_n'(qR) K_n(qr) - I_n(qr) K_n'(qR)}$$ (22)

From the inversion theorem of Laplace transformations it follows with $p \to \lambda$; $q \to \mu = \sqrt{\lambda/\varkappa}$

$$T_{n\varrho} = \frac{D_n}{2\pi i} \cdot \int_{\gamma-i\infty}^{\gamma+i\infty} \frac{e^{\lambda t}}{\lambda} \cdot \frac{I_n(\mu\varrho)K_n(\mu r) - I_n(\mu r)K_n(\mu\varrho)}{\mu[I_n'(\mu R)K_n(\mu r) - I_n(\mu r)K_n'(\mu R)]} d\lambda$$ (23)

In this formula γ has to be chosen to be so large that all singularities of the integrand are lying on the left of γ in the complex-number plane. The integral (23) can be evaluated by application of the residue theorem.

2.1.2 Simple pole at $\lambda = 0$

At $\lambda = 0$ the integrand possesses a simple pole. With the differentiation rules for Bessel functions

$$I_n'(z) = \frac{n}{z} I_n(z) + I_{n+1}(z)$$

(24a)

and
$$K_n'(z) = \frac{n}{z} K_n(z) - K_{n+1}(z)$$
(24b)

one obtains by use of asymptotic representations for low arguments

$$K_0(x) \approx \ln \frac{2}{x} \qquad\qquad K_n(x) \approx \frac{1}{2} \Gamma(n) (2/x)^n$$
(25)

$$I_0(x) \approx 1 \qquad\qquad I_n(x) \approx (x/2)^n / \Gamma(n+1)$$
(26)

the residue

$$\text{Res}\Big|_{\mu=0} = \frac{R}{\mu n} \cdot \frac{I_n(\mu\varrho)K_n(\mu r) - I_n(\mu r)K_n(\mu\varrho)}{I_n'(\mu R)K_n(\mu r) - I_n(\mu r)K_n'(\mu R)}\Big|_{\mu=0} = \frac{R}{n} \cdot \frac{(\varrho/r)^n - (r/\varrho)^n}{(R/r)^n + (r/R)^n} \qquad \text{for } n > 0,$$
(27a)

$$\text{Res}\Big|_{\mu=0} = R \cdot \ln(\varrho/r) \qquad \text{for } n = 0$$
(27b)

2.1.3 Zeroes of the nominator

Further singularities of the integrand are caused by zeroes of the nominator N

$$N = \mu [I_n'(\mu R)K_n(\mu r) - I_n(\mu r)K_n'(\mu R)] = 0$$
(28)

The singularities are lying in $\mu = i\alpha_k$, where α_k are the positive roots of the equation

(29)
$$\frac{n}{R} [Y_n(\alpha_k r) J_n(\alpha_k R) - J_n(\alpha_k r) Y_n(\alpha_k R)] - \alpha_k [Y_n(\alpha_k r) J_{n+1}(\alpha_k R) - J_n(\alpha_k r) Y_{n+1}(\alpha_k R)] = 0$$

J_n and Y_n are the Bessel functions of order n [20]. To calculate the redidues at α_k the expressions

$$\lambda \frac{dN}{d\lambda}\Big|_{\lambda = -\varkappa \alpha_k^2} = \frac{1}{2} \mu \frac{dN}{d\mu}\Big|_{\mu = i\alpha_k}$$

are necessary.

A longer analysis yields

$$\frac{dN}{d\mu}\bigg|_{\mu=i\alpha} = \mu R\left(1+\frac{n^2}{\mu^2 R^2}\right)\left[I_n(\mu R)K_n(\mu r)-I_n(\mu r)K_n(\mu R)\right]+\mu r\left[I_n'(\mu R)K_n'(\mu r)-I_n'(\mu r)K_n'(\mu R)\right] \tag{30}$$

Application of the functional equation [20]

$$I_n(z)K_n'(z)-K_n(z)I_n'(z)=-\frac{1}{z} \tag{31}$$

leads to

$$\frac{dN}{d\mu}\bigg|_{\mu=i\alpha} = -\left(\frac{n^2}{\mu^2 R^2}+1\right)\frac{I_n(\mu r)}{I_n'(\mu R)}-\frac{I_n'(\mu R)}{I_n(\mu r)} \tag{32}$$

Use of the relation between Bessel functions and modified Bessel functions

$$I_n(ix)=i^n J_n(x) \tag{33}$$

produces

$$\lambda\frac{dN}{d\lambda}\bigg|_{\lambda=\alpha\alpha_k^2} = \frac{\mu}{2}\frac{dN}{d\mu}\bigg|_{\mu=i\alpha_k} = \frac{\alpha_k}{2}\left(1-\frac{n^2}{\alpha_k^2 R^2}\right)\frac{J_n(\alpha_k r)}{J_n'(\alpha_k R)}-\frac{\alpha_k}{2}\cdot\frac{J_n'(\alpha_k R)}{J_n(\alpha_k r)} \tag{34}$$

Thereby the residues are found

$$Res\bigg|_{\alpha_k} = -e^{-\alpha\alpha_k^2 t}\pi\frac{J_n(\alpha_k R)J_n(\alpha_k r)[J_n(\alpha_k\rho)Y_n(\alpha_k r)-J_n(\alpha_k r)Y_n(\rho\alpha_k)]}{\alpha_k[(1-n^2/\alpha_k^2 R^2)J_n^2(\alpha_k r)-J_n'^2(\alpha_k R)]} \tag{35}$$

Since the value of the integral (23) is equal to the sum of residues, one obtains for $n>0$

$$T_{n\varrho} = D_n \frac{R}{n} \frac{(\varrho/r)^n - (r/\varrho)^n}{(R/r)^n + (r/R)^n} - \pi D_n \sum_{k=1}^{\infty} e^{-\varkappa \alpha_k^2 t} \frac{J_n'(\alpha_k R) J_n(\alpha_k r) [J_n(\alpha_k \varrho) Y_n(\alpha_k r) - J_n(\alpha_k r) Y_n(\alpha_k \varrho)]}{\alpha_k [(1 - n^2/\alpha_k^2 R^2) J_n^2(\alpha_k r) - J_n'^2(\alpha_k R)]} \quad (36)$$

If n = 0 -i.e. angle independence of $T_{0\varphi}$ - it results

$$T_{0\varrho} = D_0 R \ln(\varrho/r) - \pi D_0 \sum_{k=1}^{\infty} e^{-\varkappa \alpha_k^2 t} \frac{J_1(\alpha_k R) J_0(\alpha_k r) [J_0(\alpha_k \varrho) Y_0(\alpha_k r) - J_0(\alpha_k r) Y_0(\alpha_k \varrho)]}{\alpha_k [J_0^2(\alpha_k r) - J_1^2(\alpha_k R)]} \quad (37)$$

The case n = 0 is also treated in [15]. The results are in agreement. The general solution in case of heat flux distributions symmetrical to φ = 0 (only cos-terms!) is given by

$$T(\varrho, \varphi, t) = \sum_{n=0}^{\infty} T_{n\varrho}(\varrho, t) \cos n\varphi \quad (38)$$

2.2 Temperature distributions

Since the Fourier components of the temperature are known, any possible heat flux distribution symmetrical to φ = 0 can be evaluated.

The procedure will be demonstrated for a heat radiating end-less strip of width 2a and distance l from the tube centre, as shown in Fig. 2.
The flux contribution of a small strip element with the area dF′ is

$$d\dot{Q} = C \frac{\cos \vartheta \, dF'}{s} \cos(\vartheta - \varphi) = C \cos(\vartheta - \varphi) \, d\vartheta \quad (39)$$

For $\varphi \gtrless 0$ the whole intensity on the tube surface is given by

$$\dot{Q}(\varphi) = \begin{cases} C \int_{\alpha}^{\vartheta_2} \cos(\vartheta - \varphi) \, d\vartheta = C [\sin(\vartheta_2 - \varphi) - \sin(\alpha - \varphi)] & \text{for } \vartheta_2 \geqslant \alpha \\ 0 & \text{for } \vartheta_2 < \alpha \end{cases} \quad (40)$$

and $\qquad\qquad \dot{Q}(-\varphi) = \dot{Q}(\varphi)$

with $\quad \vartheta_1 = -\arctan \dfrac{a+R\sin\varphi}{1-R\cos\varphi}$

$$\alpha = \text{Max} \left\{ \vartheta_1 , \varphi - \frac{\pi}{2} \right\} \qquad (41)$$

$\vartheta_2 = \arctan \dfrac{a-R\sin\varphi}{1-R\cos\varphi}$

From Eq. (41) it results for $\varphi = 0$

$$\vartheta_1(0) = -\arctan\frac{a}{1-R} \qquad ; \qquad \vartheta_2(0) = \arctan\frac{a}{1-R}$$

so we get the maximum intensity

$$\dot{Q}(0) = 2C \left[1 + \left(\frac{1-R}{a}\right)^2 \right]^{-1/2} \qquad (42)$$

Elimination of C in Eq. (40) leads to

$$(43)$$

$$\dot{Q}(\varphi) = \begin{cases} \dot{Q}(0) \left[1 + \left(\frac{1-R}{a}\right)^2 \right]^{1/2} \left[(\sin\vartheta_2 - \sin\alpha)\cos\varphi - (\cos\vartheta_2 - \cos\alpha)\sin\varphi \right]/2 & \text{for } \vartheta_2 \geq \alpha \\ 0 & \text{for } \vartheta_2 < \alpha \end{cases}$$

The Fourier coefficients of this distribution can be determined by

$$\dot{Q}_n = \frac{1}{2\pi} \int\limits_{-\pi}^{\pi} \dot{Q}(\varphi)\cos(n\varphi)\,d\varphi \qquad (44)$$

In special cases these coefficients can be evaluated analytically.

2.2.1 Tube in front of a heat radiating semi-infinite body

This special case is characterised by $a \to \infty$.
The angles become $\quad \vartheta_1 = -\pi/2 \ , \quad \vartheta_2 = \pi/2 \quad , \quad \alpha = \varphi - \pi/2$
Introduction into Eq. (43) gives

$$\dot{Q}(\varphi) = \frac{1}{2}\dot{Q}(0)\left[(1-\sin(\varphi-\pi/2))\cos\varphi + \cos(\varphi-\pi/2)\sin\varphi\right] = \frac{1}{2}\dot{Q}(0)\left[1+\cos\varphi\right] \qquad (45)$$

The Fourier series has only two terms $(\dot{Q}_0 = \dot{Q}_1 = \dot{Q}(0)/2)$ and evaluation becomes very simple. From Eq. (4) we get the time-dependent temperature distribution. Figure 3 shows the temperature distribution for a thick-walled tube with $R/r = 2$ for $\varphi = 0, \pi/2$ and π. The temperature values are normalised to the temperature of the hottest point on the outer surface $(\varphi = 0, \varrho = R)$.

The stationary temperature distribution follows from Eqs. (36) and (37) for $t \to \infty$

$$T_\infty(\varrho, \varphi) = \frac{\dot{Q}(0)}{2} \wedge R \left[\ln \varrho/r + \frac{\varrho/r - r/\varrho}{R/r + r/R} \cos \varphi \right] \tag{46}$$

Figure 4 gives a representation of this relation in isotherms.

2.2.2 Radiation source at an infinite distance from the tube

This special case is characterised by $l \to \infty$.

Therefore, the angles ϑ_1 and ϑ_2 become very small. Because of the approximative formulas

$$\sin(\arctan x) \cong x \quad ; \quad \cos x \cong 1$$

it results from Eq. (43)

$$\dot{Q}(\varphi) = \begin{cases} \dot{Q}(0) \cos \varphi & \text{for } |\varphi| \leq \pi/2 \\ 0 & \text{for } |\varphi| > \pi/2 \end{cases} \tag{47}$$

The Fourier series of this well-known distribution is

$$\dot{Q} = \frac{\dot{Q}(0)}{\pi} \left[1 + \frac{\pi}{2} \cos \varphi + \sum_{\gamma=1}^{\infty} (-1)^{\gamma-1} \cdot \frac{2}{(2\gamma+1)(2\gamma-1)} \cos 2\gamma\varphi \right] \tag{48}$$

The stationary temperature distribution is given by

$$T(\varrho, \varphi) = \frac{\wedge \dot{Q}(0) R}{\pi} \left[\ln \frac{\varrho}{r} + \frac{\pi}{2} \frac{\varrho/r - r/\varrho}{R/r + r/R} \cos \varphi + \sum_{\gamma=1}^{\infty} \frac{(-1)^{\gamma-1}}{\gamma(2\gamma-1)(2\gamma+1)} \cdot \frac{(\varrho/r)^{2\gamma} - (r/\varrho)^{2\gamma}}{(R/r)^{2\gamma} + (r/R)^{2\gamma}} \cos 2\gamma\varphi \right] \tag{49}$$

Figure 5 represents the corresponding isotherms. The distribution across the wall is shown in Fig. 6.

2.3   Thermal stresses in the tube wall

Thermal stress calculations can be performed by application of the temperature results reported in chapter 2.2. This will be shown in detail for a tube in front of a heat radiating semi-infinite body. To simplify the notations the geometrical data are normalised to the inner radius by setting

$$r = 1.$$

Axial strains and deflections caused by bending moments should be prevented, i.e. $\varepsilon_z = 0$.
The elastic basic equations are

$$\sigma_\varrho = \frac{E}{(1+\mu)(1-2\mu)} \left[(1-\mu)\varepsilon_\varrho + \mu\varepsilon_\varphi - (1+\mu)\alpha T \right]$$

$$\sigma_\varphi = \frac{E}{(1+\mu)(1-2\mu)} \left[(1-\mu)\varepsilon_\varphi + \mu\varepsilon_\varrho - (1+\mu)\alpha T \right] \tag{50}$$

$$\sigma_{\varrho\varphi} = \frac{E}{1+\mu} \varepsilon_{\varrho\varphi}$$

where $\sigma_{\varrho\varphi}$ and $\varepsilon_{\varrho\varphi}$ are standing for the shear stress and strain, μ the Poisson's ratio, α the coefficient of expansion and E the Young's modulus.
Two equilibrium conditions are given by

$$\frac{\partial \sigma_\varrho}{\partial \varrho} + \frac{1}{\varrho} \frac{\partial \sigma}{\partial \varphi} + \frac{\sigma_\varrho - \sigma_\varphi}{\varrho} = 0$$

$$\frac{\partial \sigma_{\varrho\varphi}}{\partial \varrho} + \frac{1}{\varrho} \frac{\partial \sigma_\varphi}{\partial \varphi} + \frac{2\sigma_{\varrho\varphi}}{\varrho} = 0 \tag{51}$$

The strain components can be expressed by the displacements (u,v) in cylindrical coordinates

$$\varepsilon_\varrho = \frac{\partial u}{\partial \varrho} \quad ; \quad \varepsilon_\varphi = \frac{1}{\varrho} \frac{\partial v}{\partial \varphi} + \frac{u}{\varrho} \quad ; \quad \varepsilon_{\varrho\varphi} = \frac{1}{2} \left(\frac{1}{\varrho} \frac{\partial u}{\partial \varphi} + \frac{\partial v}{\partial \varrho} - \frac{v}{\varrho} \right) \tag{52}$$

Since the temperature distribution is given by a Fourier series
it can be concluded that the displacements are

$$u = \sum_n u_n(\varrho) \cos n\varphi \quad ; \quad v = \sum_n v_n(\varrho) \sin n\varphi \qquad (53)$$

Substitution into Eq. (52) leads to

$$\varepsilon_\varrho = \sum_n \frac{\partial u_n}{\partial \varrho} \cos n\varphi$$

$$\varepsilon_\varphi = \frac{1}{\varrho} \sum_n (n v_n + u_n) \cos n\varphi \qquad (54)$$

$$\varepsilon_{\varrho\varphi} = \frac{1}{2} \sum_n (\frac{\partial v_n}{\partial \varrho} - \frac{v_n}{\varrho} - \frac{n u_n}{\varrho}) \sin n\varphi$$

Introducing Eq. (54) into Eq. (50) and Eq. (51) one obtains a
system of two coupled differential equations

$$v_n'' \varrho + v_n' \varrho - [1 + \frac{2(1-\mu)n^2}{1-2\mu}] v_n - \frac{n}{1-2\mu} \varrho u_n' - n \frac{3-4\mu}{1-2\mu} u_n = - \frac{1+\mu}{1-2\mu} 2 \alpha \varrho n T_n \qquad (55)$$

$$u_n'' \varrho + u_n' \varrho - [1 + \frac{(1-2\mu)n^2}{2(1-\mu)}] u_n + \frac{n}{2(1-\mu)} \varrho v_n' - n \frac{3-4\mu}{2(1-\mu)} v_n = \frac{1+\mu}{1-\mu} \alpha \varrho^2 T_n'$$

The solution of this system will yield the displacements and,
using Eqs. (52) and (50), the related stresses in the tube cross-
section.

2.3.1 Displacements

Application of the general set-up

$$v = A \varrho^k \qquad u = B \varrho^k \qquad (56)$$

gives the solution of the homogeneous form of Eq. (55)

$$u = A_1 \varrho + A_2 \varrho^{-1}$$
$$v = 0$$
$$\text{for } n = 0 \qquad (57)$$

and

$$u = A_1 \frac{1-4\mu}{5-4\mu} \varrho^2 + A_2 \varrho^{-2} + (\frac{A_4}{3-4\mu} - A_3) - A_4 \ln \varrho$$

$$v = A_1 \varrho^2 + A_2 \varrho^{-2} + A_3 + A_4 \ln \varrho$$
$$\text{for } \quad n = 1 \qquad (58)$$

To get the complete solution of Eq. (55) a particular solution
of the non-homogeneous system is necessary. It can be evaluated
by the method of "variation of parameters".

For n = 0 only a single differential equation follows. Its solu-
tion is

$$u_i = \alpha \, \frac{1+\mu}{1-\mu} \, \frac{1}{\varrho} \int\limits_1^\varrho T \, \xi \, d\xi \tag{59}$$

For n = 1 the respective displacements are given by

$$u_i = \frac{1}{2} \, \frac{1+\mu}{1-\mu} \, [\frac{1}{\varrho^2} \int\limits_1^\varrho x^2 T \, dx + \int\limits_1^\varrho T \, dx - \frac{1}{8} T'(1)(\frac{1}{\varrho^2} + \frac{4}{3-4\mu} - 4 \ln \varrho - \frac{1-4\mu}{5-4\mu} \varrho^2)] \tag{60}$$

$$v_i = \frac{1}{2} \, \frac{1+\mu}{1-\mu} \, [\frac{1}{\varrho^2} \int\limits_1^\varrho x^2 T \, dx - \int\limits_1^\varrho T \, dx + \frac{1}{8} T'(1)(\varrho^2 - \frac{1}{\varrho^2} - 4 \ln \varrho)]$$

2.3.2 Stresses in the tube wall

The stresses can be computed by application of Eqs. (54) and
(50). The unknown constants A_1, A_2, A_3, A_4 have to satisfy the
boundary conditions at the outer and inner surfaces

$$\sigma_\varrho (R) = \sigma_\varrho(1) = \sigma_{\varrho\varphi}(R) = \sigma_{\varrho\varphi}(1) = 0 \tag{61}$$

For n = 0 we find

$$\sigma_{\varrho_0} = \frac{\alpha E}{1-\mu} \, [\frac{\varrho^2 -1}{R^2 -1} \, \frac{1}{\varrho^2} \int\limits_1^R T \xi \, d\xi - \frac{1}{\varrho^2} \int\limits_1^\varrho T\xi \, d\xi] \qquad \sigma_{\varrho\varphi_0} = 0 \tag{62}$$

$$\sigma_{\varphi_0} = \frac{\alpha E}{1-\mu} \, [\frac{\varrho^2 +1}{R^2 -1} \, \frac{1}{\varrho^2} \int\limits_1^R T\xi \, d\xi + \frac{1}{\varrho^2} \int\limits_1^\varrho T\xi \, d\xi - T]$$

and for n = 1 the following expressions hold

$$\sigma_{\varrho_1} = \frac{\alpha E}{1+\mu} \, [\frac{2}{5-4\mu} A_1 \varrho - 2A_2 \varrho^{-3} - \frac{3-2\mu}{3-4\mu} A_4 \varrho^{-1}] + \frac{\alpha E}{1-\mu} \, (\frac{1}{8} \frac{\partial T}{\partial \varrho}(1)(\varrho^{-3} + \frac{6-4\mu}{3-4\mu} \varrho^{-1} + \frac{1}{5-4\mu} \varrho) - \frac{1}{\varrho^3} \int\limits_1^\varrho \xi^2 T d\xi)$$

$$\tag{63}$$

$$\sigma_{\varphi_1} = \frac{\alpha E}{1+\mu} \, [\frac{2}{5-4\mu} A_1 \varrho - 2A_2 \varrho^{-3} + \frac{1-2\mu}{3-4\mu} A_4 \varrho^{-1}] + \frac{\alpha E}{1-\mu} \, (\frac{1}{8} \frac{\partial T}{\partial \varrho}(1)(\varrho^{-3} + \frac{6-4\mu}{3-4\mu} \varrho^{-1} + \frac{1}{5-4\mu} \varrho) - \frac{1}{\varrho^3} \int\limits_1^\varrho \xi^2 T d\xi)$$

$$\sigma_{r_1} = \frac{\alpha E}{1+\mu} \, [\frac{6}{5-4\mu} A_1 \varrho + 2A_2 \varrho^{-3} + \frac{1-2\mu}{3-4\mu} A_4 \varrho^{-1}] + \frac{\alpha E}{1-\mu} \, (\frac{1}{8} \frac{\partial T}{\partial \varrho}(1)(\frac{3}{5-4\mu} \varrho - \varrho^{-3} - \frac{2-4\mu}{3-4\mu} \varrho^{-1}) + \frac{1}{\varrho^3} \int\limits_1^\varrho \xi^2 T d\xi) - \alpha \frac{ET}{1-\mu}$$

with

$$A_1 = -\frac{1}{2}\frac{1+\mu}{1-\mu}\left[\frac{1}{8}\frac{\partial T}{\partial \varrho}(1) - (5-4\mu)\frac{\int_1^R \xi^2 T\, d\xi}{R^4 - 1}\right]$$

$$A_2 = \frac{1}{2}\frac{1+\mu}{1-\mu}\left[\frac{1}{8}\frac{\partial T}{\partial \varrho}(1) + \frac{\int_1^R \xi^2 T\, d\xi}{R^4 - 1}\right]$$

$$A_4 = \frac{1}{4}\frac{1+\mu}{1-\mu}\frac{\partial T}{\partial \varrho}(1)$$

Taking into account the first terms of Eqs. (36) and (37) the stationary stress components, after dropping the restriction r = 1 (i.e. R $\longrightarrow$ R/r and ρ $\longrightarrow$ ρ/r), can be written as

$$\sigma_{\varrho_0} = \frac{1}{4}\frac{\alpha E}{1-\mu}\Lambda\,\dot{Q}_0 R\left[\frac{\varrho^2-r^2}{R^2-r^2}\frac{1}{\varrho^2}(2R^2\ln\frac{R}{r}-R^2+r^2) - 2\ln\frac{\varrho}{r} - \frac{r^2}{\varrho^2} + 1\right]$$

$$\sigma_{\varphi_0} = \frac{1}{4}\frac{\alpha E}{1-\mu}\Lambda\dot{Q}_0 R\left[\frac{\varrho^2+r^2}{R^2-r^2}\frac{1}{\varrho^2}(2R^2\ln\frac{R}{r}-R^2+r^2) - 2\ln\frac{\varrho}{r} + \frac{r^2}{\varrho^2} - 1\right] \tag{64}$$

$$\sigma_{\varrho\varphi_0} = 0 \quad ; \quad \sigma_{z_0} = \mu(\sigma_{\varrho_0}-\sigma_{\varphi_0}) - \alpha E\Lambda\dot{Q}_0 R\ln\frac{\varrho}{r}$$

and

$$\sigma_{\varrho_1} = \frac{1}{2}\frac{\alpha E}{1-\mu}\dot{Q}_1\Lambda R\left[\frac{r}{\varrho} - \frac{\varrho\,r}{r^2+R^2} - \frac{R^2}{R^2+r^2}(r/\varrho)^3\right]$$

$$\sigma_{\varphi_1} = \frac{1}{2}\frac{\alpha E}{1-\mu}\dot{Q}_1\Lambda R\left[\frac{r}{\varrho} - 3\frac{\varrho\,r}{r^2+R^2} + \frac{R^2}{R^2+r^2}(r/\varrho)^3\right] \tag{65}$$

$$\sigma_{\varrho\varphi_1} = \sigma_{\varrho_1}$$

$$\sigma_{z_1} = \mu(\sigma_{\varrho_1}+\sigma_{\varphi_1}) - \alpha E\Lambda\dot{Q}_1 R\left(\frac{\varrho}{r}-\frac{r}{\varrho}\right)/\left(\frac{R}{r}+\frac{r}{R}\right)$$

Then the stresses are given by

$$\sigma_{\varrho} = \sigma_{\varrho_0} + \sigma_{\varrho_1}\cos\varphi$$
$$\sigma_{\varphi} = \sigma_{\varphi_0} + \sigma_{\varphi_1}\cos\varphi$$
$$\sigma_{\varrho\varphi} = \sigma_{\varrho\varphi_0} + \sigma_{\varrho\varphi_1}\sin\varphi \tag{66}$$

For a tube in front of a heat radiating semi-infinite body $\dot{Q}_0 = \dot{Q}_1 = \dot{Q}/2$. By use of Eqs. (36), (37), (62) and (63) the in-

stationary stresses can be evaluated. Figure 7 shows the circumferential stresses σ_φ as a function of the normalised time for a thick-walled tube (R = 2r). Maximum stress values are reached in the stationary case. Figure 8 represents the stationary stress distributions for σ_φ, σ_ρ, $\sigma_{\rho\varphi}$ and different values of φ. It is well known that temperature components T_n with n > 1 have no influence on stationary stresses in tubes [21]. So it is possible to compose all stationary stress distributions by use of the components with n = 0 and n = 1.

Figure 9 shows the circumferential stresses in a tube heated by a radiation source placed at an infinite distance.

2.4 Stationary temperature distributions for additional volumetric heating

Due to the fast neutrons (14 MeV) occuring in fusion reactors a volumetric heat production in the tube wall has to be taken into account. If $\dot{q}$ is the density of the heat production rate the stationary heat conduction equation can be written as

$$\Delta T + \Lambda \dot{q} = 0 \tag{67}$$

A general solution of this equation is not possible. A set-up similar to Eq. (7) gives no spearation of the variables ρ and φ. Therefore, only two important special cases for $\dot{q}(\rho, \varphi)$ are investigated. Because absorption of neutrons in steel is relative small, $\dot{q}$ can be considered as independent of ρ, i.e.

$$\dot{q} \neq f(\rho) \tag{68}$$

2.4.1 Constant heat production in the tube wall

The simplest assumption is a constant heat production in the tube wall

$$\dot{q} = const.$$

This case can be assumed if absorption in the coolant medium is also small. Equation (67) can be written

$$\frac{1}{\varrho}\frac{\partial T}{\partial \varrho} + \frac{\partial^2 T}{\partial \varrho^2} + \frac{1}{\varrho^2}\frac{\partial^2 T}{\partial \varphi^2} + \Lambda \dot{q} = (\frac{1}{\varrho}\frac{\partial T}{\partial \varrho} + \frac{\Lambda \dot{q}}{2}) + (\frac{\partial^2 T}{\partial \varrho^2} + \frac{\Lambda \dot{q}}{2}) + \frac{1}{\varrho^2}\frac{\partial^2 T}{\partial \varphi^2} = 0 \qquad (69)$$

and because of $\dot{q} \neq f(\varphi)$

$$\frac{1}{\varrho}\frac{\partial (T + \varrho^2 \Lambda \dot{q}/4)}{\partial \varrho} + \frac{\partial^2 (T + \varrho^2 \Lambda \dot{q}/4)}{\partial \varrho^2} + \frac{1}{\varrho^2}\frac{\partial^2 (T + \varrho^2 \Lambda \dot{q}/4)}{\partial \varphi^2} = 0 \qquad (70)$$

By substitution

$$\Theta = T + \varrho^2 \Lambda \dot{q}/4 \qquad (71)$$

it results

$$\Delta \Theta = 0 \qquad (72)$$

The solution of this equation leads to $\Theta \sim \ln(\varrho/r)$. By superimposition of the solution of Eq. (37) for surface heating and consideration of the boundary conditions in Eqs. (3) and (4) one obtains

$$T = Q_0 \Lambda R \ln \frac{\varrho}{r} + \frac{1}{2} R^2 \Lambda \dot{q} \ln \frac{\varrho}{r} - \frac{1}{4} \Lambda \dot{q}(\varrho^2 - r^2) \qquad (73)$$

The relation in Eq. (73) is depicted in Fig. 10 for different values of $R \cdot \dot{q}/\dot{Q}$.

2.4.2 φ-dependent heat production in the tube wall

If absorption in the coolant medium is worth mentioning the rear parts of the thin-walled tube will become partially shielded from neutron radiation. Therefore, an angle dependency of $\dot{q}$ has to be taken into account. The Fourier series of the heat

production rate holds

$$\dot{q} = \sum_{n=0}^{\infty} \dot{q}_n \cos(n\varphi) \tag{74}$$

For the temperature distribution one has also to expect a Fourier series

$$T(\varrho,\varphi) = \sum_{n=0}^{\infty} T_n(\varrho) \cos(n\varphi) \tag{75}$$

Introduction of Eqs. (74) and (75) into Eq. (67) yields

$$\frac{\partial^2 T_n}{\partial \varrho^2} + \frac{1}{\varrho} \frac{\partial T_n}{\partial \varrho} - \frac{n^2}{\varrho^2} T_n + \Lambda \dot{q}_n = 0 \tag{76}$$

From the homogeneous differential equation it results

$$\frac{1}{\Lambda} T_{n_{hom}} = A_n \varrho^n + B_n \varrho^{-n} \qquad \text{for} \quad n>0 \tag{77}$$

$$\frac{1}{\Lambda} T_{0_{hom}} = A_0 \ln \varrho + B_0 \qquad \text{for} \quad n=0$$

A particular solution of the inhomogeneous equation can be found with the set-up

$$\frac{1}{\Lambda} T_{n_{inh}} = C_n \dot{q}_n \varrho^2 \tag{78}$$

Introduced into Eq. (76) it results in

$$C_n = \frac{1}{n^2 - 4} \qquad \text{for} \quad n \neq 2 \tag{79}$$

and

$$\frac{1}{\Lambda} T_{n_{inh}} = \frac{1}{n^2 - 4} \dot{q}_n \varrho^2 \tag{80}$$

For n = 2 one obtains by the method of "variation of para-
meters"

$$\frac{1}{\Lambda} T_{n_{inh}} = -\frac{1}{4} \dot{q}_n \varrho^2 \ln \varrho \tag{81}$$

By superposition of homogeneous and inhomogeneous solutions
the total solution is given by

$$\frac{1}{\Lambda} T = A_0 \ln \varrho + B_0 - \frac{1}{4} \dot{q}_0 \varrho + (A_2 \varrho^2 + \frac{B_2}{\varrho^2} - \frac{1}{4} \dot{q}_2 \varrho^2 \ln \varrho) \cos 2\varphi$$

$$+ \sum_{\substack{n=1 \\ (n \neq 2)}}^{\infty} (A_n \varrho^n + \frac{B_n}{\varrho^n} - \frac{\dot{q}_n}{4-n^2} \varrho^2) \cos n\varphi \tag{82}$$

From the boundary condition in Eq. (3) at the inner surface
($\varrho = r$) one obtains

$$B_n = \frac{\dot{q}_n}{4-n^2} r^{n+2} - A_n r^{2n} \qquad n \neq 2$$

$$B_2 = \frac{\dot{q}_2}{4} r^4 \ln r - A_2 r^4 \tag{83}$$

and from the boundary condition in Eq. (4) it can be concluded

$$A_0 = \dot{Q}_0 R + \frac{1}{2} \dot{q}_0 R^2$$

$$A_2 = \frac{\dot{Q}_2}{2R} + \frac{B_2}{R^4} + \frac{1}{4} \dot{q}_2 (\ln R + \frac{1}{2})$$

$$A_n = \frac{\dot{Q}_n}{n R^{n-1}} + \frac{B_n}{R^{2n}} + \frac{2\dot{q}_n}{n(4-n^2)} R^{2-n} \tag{84}$$

By combination of Eqs. (83) and (84) A_n and B_n can be deter-
mined as

$$A_0 = \dot{Q}_0 R + \frac{1}{2} \dot{q}_0 R^2$$

$$A_2 = \frac{\dot{Q}_2 R^3 + \dot{q}_2 R^4 (\ln R + 1/2)/2 + \dot{q}_2 r^4 (\ln r)/2}{2R^4 + 2r^4}$$

$$A_n = \frac{\frac{1}{n} R^{n+1} (\dot{Q}_n + \frac{2\dot{q}_n}{4-n^2} R) + \frac{\dot{q}_n}{4-n^2} r^{2+n}}{R^{2n} + r^{2n}} \tag{85}$$

and
$$B_0 = - \dot{Q}_0 R \ln r - \frac{1}{2} \dot{q}_0 R^2 \ln r + \frac{1}{4} \dot{q}_0 r^2$$

$$B_2 = \frac{\frac{\dot{q}_2}{4} r^4 R^4 \ln(r/R) - \frac{\dot{q}_2}{8} R^4 r^4 - \frac{\dot{Q}_2}{2} r^4 R^3}{R^4 + r^4} \tag{86}$$

$$B_n = \frac{\frac{\dot{q}_n}{4-n^2} r^{2+n} R^{2n} - \frac{1}{n} R^{n+1} r^{2n} (\dot{Q}_n + \frac{2 \dot{q}_n}{4-n^2} R)}{R^{2n} + r^{2n}}$$

For n = 0 the results of Eq. (73) and Eqs. (82, 84, 85, 86) are identical. Figure 10 b shows for this case how the shape of the temperature distribution changes with increasing portion of volumetric heating. In this representation the value $R\dot{q}_0/\dot{Q}_0 = 0$ is standing for pure surface heating and $R\dot{q}_0/\dot{Q}_0 \rightarrow \infty$ for pure volumetric heating.

2.5 Stationary temperature in non-concentric tubes

In the previous analysis only tubes with concentric circular cross sections were examined. For tubes directly affected by the plasma a change in tube wall thickness caused by sputtering has to be expected. Wall regions at the front side ($\varphi \approx 0$) become thinner than regions at the rear side ($\varphi \approx \pi/2$). Therefore, a temperature distribution results which deviates from that of concentric tubes. An analytical solution is possible in case of an eccentric circular tube.

2.5.1 Analysis of an eccentric circular tube

At first a tube situated in front of a radiating half-space is regarded. The rate of sputtering should be assumed to be subjected to the same dependency as the heat radiation distribution so that in a first approximation a nearly eccentric tube will result. The correct shape of the tube wall will become more complex since sputtering is not only dependent on the in-

tensity but also on the angle of incidence of corpuscular radiation. Another reason for the occurrence of eccentric tubes results from the intention to build a sacrificial layer in regions subjected to high sputtering. The special case of an arbitrarily given temperature on the outer surface and T = 0 on the inner surface is treated in [15]. The geometrical units of such a wall are given in Fig. 11 a in bipolar coordinates with the focus distance 2l. The bipolar radii of any point of the tube wall are ϱ_1 and ϱ_2 the corresponding angles θ_1 and θ_2. R_1 and R_2 are standing for points on the outer circle, r_1 and r_2 for points on the inner circle. With the abbreviation

$$\eta = \theta_1 - \theta_2 \tag{87}$$

It results for a temperature distribution symmetrical to $\eta = 0$

$$T = \sum_{n=0}^{\infty} \frac{\left(\frac{r_2 \varrho_1}{r_1 \varrho_2}\right)^n - \left(\frac{r_1 \varrho_2}{r_2 \varrho_1}\right)^n}{\left(\frac{r_2 R_1}{r_1 R_2}\right)^n - \left(\frac{r_1 R_2}{r_2 R_1}\right)^n} \, a_n \cos(n\eta) \tag{88}$$

where

$$a_0 = \frac{1}{2\pi} \int_{-\pi}^{\pi} T(\eta') \, d\eta' \tag{89}$$

$$a_n = \frac{1}{\pi} \int_{-\pi}^{\pi} T(\eta') \cos(n\eta') \, d\eta'$$

are the coefficients in the Fourier series for $T(\eta)$ in the interval $-\pi$ to π. The introduction of polar coordinates (ϱ, φ) with the origin in the centre of the outer circle is shown in Fig. 11 b. If the distance of both circle centres is D, the distance $\varkappa$ of the origin of polar coordinates from the directly adjacent focus of the bipolar coordinate system is given by

$$\varkappa = \sqrt{R^2 + l^2} - l \tag{90}$$

and l is defined as

$$l = \sqrt{\left(\frac{R^2 - r^2 - D^2}{2D}\right)^2 - r^2} \qquad (91)$$

The quotients R_1/R_2, r_1/r_2 and ϱ_1/ϱ_2 in Eq. (88) can be replaced by

$$\frac{\varrho_1}{\varrho_2} = \frac{\varrho + \sqrt{\varrho^2 + l^2} - l}{\varrho + \sqrt{\varrho^2 + l^2} + l} \qquad (92.1)$$

$$\frac{r_1}{r_2} = \frac{r + \sqrt{r^2 + l^2} - l}{r + \sqrt{r^2 + l^2} + l} \qquad (92.2)$$

$$\frac{R_1}{R_2} = \frac{R + \sqrt{R^2 + l^2} - l}{R + \sqrt{R^2 + l^2} + l} \qquad (92.3)$$

Finally, the dependency between the angles η and φ is determined as

$$\eta = A(\varrho, \varphi) = \arcsin\left[\frac{\sin\varphi}{\sqrt{1 + (\varkappa/\varrho)^2 - \frac{2\varkappa}{\varrho}\cos\varphi}}\right] - \arcsin\left[\frac{\sin\varphi}{\sqrt{1 + (\frac{2l + \varkappa}{\varrho})^2 - \frac{2(2l + \varkappa)}{\varrho}\cos\varphi}}\right] \qquad (93)$$

Equation (88) is only suitable for a given temperature distribution on the outer surface. For a given heat flux Eq. (88) has to be modified. Considering that curves with η = const are rectangular to the outer circle differentiation with respect to ϱ yields

$$\frac{dT}{d\varrho}\bigg|_{\varrho = R} = \frac{\partial T}{\partial(\varrho_1/\varrho_2)}\bigg|_R \frac{d(\varrho_1/\varrho_2)}{d\varrho}\bigg|_R = \frac{d(\varrho_1/\varrho_2)}{d\varrho}\bigg|_R \frac{R_2}{R_1} \sum_{n=0}^{\infty} n a_n \frac{\varsigma^n + \varsigma^{-n}}{\varsigma^n - \varsigma^{-n}} \cos n\eta \quad ; \quad \varsigma = \frac{r_2 R_1}{r_1 R_2} \qquad (94)$$

It should be noted that there is no singularity for n = 0 because

$$\lim_{n \to 0} \frac{n}{x^n - x^{-n}} = \frac{1}{2 \ln x} \tag{95}$$

From Eq. (92.1) one obtains

$$\frac{d(\varrho_1/\varrho_2)}{d\varrho}\bigg|_{\varrho=R} = 2/R_2^2 \tag{96}$$

and with this

$$\frac{dT}{d\varrho}\bigg|_{\varrho=R} = \frac{2}{R_1 R_2} \sum_{n=0}^{\infty} n \, a_n \frac{\zeta^n + \zeta^{-n}}{\zeta^n - \zeta^{-n}} \cos n\eta = \sum_{n=0}^{\infty} b_n \cos n\eta \tag{97}$$

$$\zeta = \frac{r_2 R_1}{r_1 R_2}$$

The Fourier coefficients b_n have to be determined from the condition for the heat flux distribution

$$\Lambda \dot{Q}(\varphi) = \sum_{n=0}^{\infty} c_n \cos n\varphi = \sum_{n=0}^{\infty} b_n \cos n\eta \tag{98}$$

where C_n are the coefficients of the heat flux distribution in polar coordinates and b_n the coefficients in bipolar coordinates. The coefficients a_n can be replaced by

$$a_n = \frac{b_n R_1 R_2}{2n} \frac{\zeta^n - \zeta^{-n}}{\zeta^n + \zeta^{-n}} \tag{99}$$

Finally, one obtains

$$T = \sum_{n=0}^{\infty} \frac{\chi^n - \chi^{-n}}{\zeta^n + \zeta^{-n}} \frac{b_n}{n} \left[\sqrt{R^2 + l^2} - R \cos \varphi \right] \frac{R}{l} \cos(n\eta) \tag{100}$$

$$\chi = (r_2 \varrho_1)/(r_1 \varrho_2)$$

where φ is given by Eq. (93)

$$\varphi = A^{-1}(R, \eta) \tag{101}$$

The maximum surface temperature is

$$\tag{102}$$

$$T(\varrho = R, \varphi = 0) = \sum_{n=0}^{\infty} \tanh\left[\, n \cdot \ln X \,\right] \frac{b_n R}{n\, I} \left(\, \sqrt{R^2 + I^2} - R \cos\varphi \,\right)$$

Figure 12 represents isotherms of a thick-walled eccentric tube. The heat flux distribution is given by Eq. (47). All temperatures are normalised to the maximum surface temperature $T(\varrho = R, \varphi = 0)$.

2.5.2 Approximation for non-circular tubes

For more complicate cross sections an analytical solution seems impossible. In such cases an approximative method will essentially simplify this problem. We assume that the temperature distribution in an arbitrarily shaped tube wall with local thickness $h(\varphi)$ will be equal to the temperature distribution in a concentric tube with the same thickness, i.e. the wall thickness for an arbitrary point has to be determined and then the temperature calculated by application of Eqs. (36), (37) and (38). To prove this method of approximation computations were performed for an eccentric tube with exact formulae and a method of approximation was applied. Thick-walled tubes with high eccentricity were chosen because maximum deviations between both methods could be expected. The relative deviations

$$\frac{\Delta T}{T_{max}} = \frac{T_{exact} - T_{approx}}{T(\varrho = R, \varphi = 0)_{exact}}$$

are depicted in Fig. 13 for $\varphi = 0$ and $\varphi = \pi$ and different values of r/R and D/R.

Since in all cases the deviations are lower than ± 4,0 %,
the proposed method seems to be a very good approximation.

3. Distribution of neutron radiation in the tube wall

Neutron radiation affects the thermal state by volumetric heat
production, gives rise to swelling and irradiation creep, and
influences the strength data by irradiation embrittlement.
Therefore, the knowledge of the distribution of neutron radi-
ation in the tube wall is necessary for realistic calculations.
In practice where the absorption in tube and breeder materials
is not negligible a complex distribution will result.

The path of a neutron beam and its geometrical data are shown
in Fig. 14. The problem is to calculate the absorption along
the path components b_1, b_2 in the tube material and a in bree-
der material up to the point (φ, ϱ). Introduction of the geo-
metrical quantity

$$\beta = \pi - \varphi + \vartheta \tag{103}$$

gives

$$\cos \beta = \frac{b_2 + a/2}{\varrho} \tag{104}$$

By application of simple geometrical theorems one obtains

$$b_2 (a + b_2) = \varrho^2 - r^2 \tag{105}$$

from the secant theorem for the outer circle, and

$$(b_1 - b_2)(b_1 + a + b_2) = R^2 - \varrho^2 \tag{106}$$

from the chord theorem for the inner circle.
Combination of Eqs. (104) and (105) yields

$$b_2 = \varrho \cos\beta - \sqrt{r^2 - \varrho^2 \sin^2\beta} \tag{107}$$

and from Eqs. (104) and (107) one obtains

$$a = 2 \sqrt{r^2 - \varrho^2 \sin^2 \beta} \qquad (108)$$

Inserting of Eqs. (107) and (108) into Eq. (106) gives

$$b_1 = \sqrt{R^2 - \varrho^2 \sin^2 \beta} \; - \sqrt{r^2 - \varrho^2 \sin^2 \beta} \qquad (109)$$

and thereby all path components are known.

3.1   Distribution in case of parallel neutron radiation

Because of symmetry with respect to $\varphi = 0$ only the right half of the tube will be treated. For parallel neutron radiation we have to put

$$\vartheta = 0 \quad ; \quad \beta = \pi - \varphi$$

For points with $\varrho^2 \sin^2 \beta \leq r^2$ it results from Eqs. (107) and (109)

$$b = b_1 + b_2 = \varrho \cos \beta + \sqrt{R^2 - \varrho^2 \sin^2 \beta} \; - 2\sqrt{r^2 - \varrho^2 \sin^2 \beta} \qquad (110)$$

and

$$a = 2 \sqrt{r^2 - \varrho^2 \sin^2 \beta}$$

In case of $\varrho^2 \sin^2 \beta > r^2$ or $\varphi < \pi/2$ we obtain

$$b = b_1 + b_2 = \varrho \cos \beta + \sqrt{R^2 - \varrho^2 \sin^2 \beta}$$
$$a = 0 \qquad (111)$$

If α_1 and α_2 are the coefficients of absorption in the breeder material and in the tube wall respectively the neutron intensity ϕ can be calculated by

$$\phi(\varrho,\varphi) = \begin{cases} \phi_0 \exp[-\alpha_2(\varrho \cos\beta + \sqrt{R^2 - \varrho^2 \sin^2\beta}\,)] & \text{for } \varphi - \pi + \arcsin\frac{r}{\varrho} < 0 \\ & \varphi < \pi/2 \\ \phi_0 \exp[-\alpha_2(\varrho \cos\beta + \sqrt{R^2 - \varrho^2 \sin^2\beta} - 2\sqrt{r^2 - \varrho^2 \sin^2\beta}\,) - \alpha 2\sqrt{r^2 - \varrho^2 \sin^2\beta}\,] \end{cases} \quad (112)$$

Figure 15 shows the distribution of neutron intensity calculated by Eq. (112) for $\varrho = r$ and $\varrho = R$ under assumption that $\alpha_2 \to 0$.

3.2 Distribution in case of a tube in front of a neutron radiating half-space

The share of radiation at the point (ϱ, φ) coming from a strip of the half-space with area dF' is

$$d\phi = C\,\frac{dF'\cos\gamma}{s} = C\,\frac{dF}{s} = C\,d\gamma \qquad (113)$$

The geometrical units can be taken from Fig. 2. In the absence of absorbend material, integration with respect to all directions of incidence gives

$$\phi_0 = C \int_{-\pi/2}^{\pi/2} d\gamma = C\,\pi \qquad C = \phi_0/\pi \qquad (114)$$

and finally

$$d\phi = \frac{\phi_0}{\pi}\,d\gamma \qquad (115)$$

If a beam crosses n absorbent layers with different coefficients of absorption and a_i is the thickness of the i-th layer the intensity of neutron radiation is given by

$$\phi = \frac{\phi_0}{\pi} \int_{-\pi/2}^{\pi/2} \exp\left[-\sum_{i=1}^{n} \alpha_i a_i(\gamma)\right] d\gamma \qquad (116)$$

Introduction of angle β (Eq. (103)) yields

$$\phi = \frac{\phi_0}{\pi} \int\limits_{\pi/2-\varphi}^{3\pi/2-\varphi} \exp\left[-\sum_{i=1}^{n} \alpha_i\, a_i(\beta)\right] d\beta \tag{117}$$

Applied to the tube with the coefficient α_1 in the breeder material and to α_2 in tube wall, this gives

a) For $\varrho \cos\varphi \leq -r$

$$\pi\frac{\phi(\varrho,\varphi)}{\phi_0} = \int\limits_{\frac{\pi}{2}-\varphi}^{-\arcsin\frac{r}{\varrho}} \exp\left[-\alpha_2(\varrho\cos\beta + \sqrt{R^2 - \varrho^2\sin^2\beta})\right] d\beta \;+$$

$$+ \int\limits_{-\arcsin\frac{r}{\varrho}}^{\arcsin\frac{r}{\varrho}} \exp\left[-\alpha_2(\varrho\cos\beta + \sqrt{R^2 - \varrho^2\sin^2\beta} - 2\sqrt{r^2-\varrho^2}\sin^2\beta) - 2\alpha_1\sqrt{r^2-\varrho^2\sin^2\beta}\right] d\beta$$

$$+ \int\limits_{\arcsin\frac{r}{\varrho}}^{\frac{3}{2}\pi-\varphi} \exp\left[-\alpha_2(\varrho\cos\beta + \sqrt{R^2 - \varrho^2\sin^2\beta})\right] d\beta \tag{118}$$

b) For $|\varrho\cos\varphi| < r$

$$\pi\frac{\phi(\varrho,\varphi)}{\phi_0} = \int\limits_{\frac{\pi}{2}-\varphi}^{\arcsin\frac{r}{\varrho}} \exp\left[-\alpha_2(\varrho\cos\beta + \sqrt{R^2 - \varrho^2\sin^2\beta} - 2\sqrt{r^2-\varrho^2}\sin^2\beta) - 2\alpha_1\sqrt{r^2-\varrho^2\sin^2\beta}\right] d\beta$$

$$+ \int\limits_{\arcsin\frac{r}{\varrho}}^{\frac{3}{2}\pi-\varphi} \exp\left[-\alpha_2(\varrho\cos\beta + \sqrt{R^2 - \varrho^2\sin^2\beta})\right] d\beta \tag{119}$$

c) For $\varrho\cos\varphi \geq r$

$$\pi\frac{\phi(\varrho,\varphi)}{\phi_0} = \int\limits_{\frac{\pi}{2}-\varphi}^{\frac{3}{2}\pi-\varphi} \exp\left[-\alpha_2(\varrho\cos\beta + \sqrt{R^2 - \varrho^2\sin^2\beta})\right] d\beta \tag{120}$$

These relations become simple if absorption in the tube wall can be neglected relative to absorption in breeder material;

i.e. $\alpha_2 << \alpha_1$. In the following we put $\alpha_2 = 0$.
By introduction of the function

$$H(\lambda,\mu,\beta) = \frac{1}{\pi} \int\limits_{0}^{\beta} \exp\left[-\lambda\sqrt{1-\mu^2\sin^2\beta'}\right] d\beta' \tag{121}$$

the simplified distribution can be written

a) If $\rho\cos\varphi \leq r$

$$\tag{122}$$

$$\phi/\phi_0 = H(2\alpha_1 r, \frac{\rho}{r}, \arcsin\frac{r}{\rho}) - H(2\alpha_1 r, \frac{\rho}{r}, -\arcsin\frac{r}{\rho}) + 1 - \frac{2}{\pi}\arcsin\frac{r}{\rho}$$

b) If $|\rho\cos\varphi| < r$

$$\phi/\phi_0 = H(2\alpha_1 r, \frac{\rho}{r}, \arcsin\frac{r}{\rho}) - H(2\alpha_1 r, \frac{\rho}{r}, \frac{\pi}{2}-\varphi) - \frac{3}{2} - \frac{\varphi}{2} - \frac{1}{\pi}\arcsin\frac{r}{\rho} \tag{123}$$

c) If $\rho\cos\varphi \geq r$

$$\phi/\phi_0 = 1 \tag{124}$$

The integral, defined in Eq. (121), has to be evaluated numerically. For a thin-walled tube the intensity distribution of neutron radiation in the wall can be represented with an acceptable accuracy by the intensity at the inner surface $\rho = r$. In this case an analytical solution of Eq. (121) is possible. One obtains

$$\tag{125}$$

$$H(\lambda,1,\beta) = \frac{1}{\pi}\int\limits_{0}^{\beta} e^{-\lambda\cos\beta'} d\beta' = \frac{1}{\pi}\int\limits_{0}^{\beta}\sum_{n=0}^{\infty}\frac{(-\lambda\cos\beta')^n}{n!} d\beta' = \frac{1}{\pi}\sum_{n=0}^{\infty}\frac{(-\lambda)^n}{n!}\int\limits_{0}^{\beta}\cos^n\beta' d\beta'$$

with the result [22]

$$H(\lambda,1,\beta) = \frac{1}{\pi} \sum_{n=0}^{\infty} \frac{(-\lambda)^n}{n!} \left(\sin\beta \sum_{\gamma=1}^{\varkappa} \frac{(n-1;-2;\gamma-1)}{(n;-2;\gamma)} \cos^{n-2\gamma+1}\beta + \frac{(1-s;2;\varkappa)}{(2-s;2;\varkappa)}\beta \right) \tag{126}$$

where $n = 2\varkappa - s$; $s = \begin{cases} 0 \\ 1 \end{cases}$ so that $\varkappa$ becomes an integer.

In Fig. 16 and 17 the intensity distributions calculated by
Eqs. (122-124) are represented for $\alpha_1 r = 0.5/1/2$ and ∞ .
In the special case of a strongly absorbing tube content
(or large inner radius); i.e. $\alpha_1 r \to \infty$, the analytical solu-
tion becomes very simple, because of

$$\phi/\phi_0 = \begin{cases} 1 - \frac{2}{\pi} \, \text{arc} \, \sin \frac{r}{\varrho} & \text{for } \varrho \cos\varphi \leq r \\ \frac{3}{2} - \frac{\varphi}{\pi} - \frac{1}{\pi} \, \text{arc} \, \sin \frac{r}{\varrho} & \text{for } |\varrho \cos\varphi| < r \\ 1 & \text{for } \varrho \cos\varphi > r \end{cases} \tag{127}$$

4. Swelling and irradiation creep

Neutron irradiation gives rise to two important phenomena
of deformation in metals, void swelling and irradiation creep.

Swelling:

The basic effect is the displacement of atoms from their
lattice sites, thus producing vacancies and interstitials. Such
defects can interact in two ways. Vacancies and interstitials
can recombine to annihilate each other, or vacancies can nucle-
ate and grow, producing so-called cavities or "voids". By the
latter process the volume of the material will increase. The
effect of volume expansion is called "swelling", abbreviated
S, and given by

$$S = \Delta V/V \tag{128}$$

Swelling is dependent on the temperature and the irradiation dose ϕt . Void swelling is strongly temperature dependent with maximum values in the range of 500 - 600°C for stainless steel, as can be seen from Fig. 18. The insert in Fig. 18 shows the dose dependency schematically. There exists an incubation dose τ_s with an approximately linear dependency. An empirical expression known from fast breeder technology is [6]

$$S(t) = R \left[\phi t + \frac{1}{\alpha} \ln \left(\frac{1 + e^{\alpha(\tau - \phi t)}}{1 + e^{\alpha \tau}} \right) \right]$$

(129)

$$R(T) = 0.002 \, \exp \left[0.042 + 1.498\beta + 0.122\beta^2 - 0.332\beta^3 - 0.441\beta^4 \right] \qquad dpa^{-1}$$

$$\tau_s = 5 \, (4.742 - 0.2326\beta + 2.717\beta^2) \qquad dpa$$

$$\alpha_s = 0.15 \qquad dpa^{-1}$$

$$\beta = (T - 500)/100 \qquad T \text{ in } °C$$

Irradiation creep

A metal subjected to neutron irradiation and non-hydrostatic stresses shows an effect of inelastic deformation, the so-called "irradiation creep". Models were developed to explain the mechanisms [23, 24] .
Neglecting a correlation between irradiation creep and swelling, the creep law can be expressed by

$$\varepsilon_{ij_c} = \frac{3}{2} C \phi S_{ij}$$

(130)

where S_{ij} is the stress deviator, which for thin-walled tubes becomes

$$S_{11} = S_z \cong \frac{2}{3}\left(\sigma_z - \frac{1}{2}\sigma_\varphi\right)$$

$$S_{22} = S_\varphi \cong \frac{2}{3}\left(\sigma_\varphi - \frac{1}{2}\sigma_z\right)$$

$$S_{33} = S_\varrho \cong 0$$

(131)

The factor of proportionality is

$$C \approx 1{,}5 \cdot 10^{-6} \quad MPa^{-1} \quad dpa^{-1}$$

(132)

for various austenitic stainless steels [25, 26]. In the interesting temperature range of $T < 550^\circ C$ thermal creep can be neglected.

5. Stress development with respect to time

5.1 Derivation of the differential equations for constant operation

The total deformation ε of a volume element in the tube wall can be composed by elastic strain ε_{el}, thermal strain ε_{th}, creep strain ε_c and deformation due to swelling ε_s, as

$$\varepsilon = \varepsilon_{el} + \varepsilon_{th} + \varepsilon_c + \varepsilon_s$$

(133)

and from this results

$$\varepsilon_z = \frac{\sigma_z}{E} - \mu\frac{\sigma_\varphi}{E} + \alpha T + B\int_0^t \left(\sigma_z - \frac{1}{2}\sigma_\varphi\right)dt + \frac{1}{3}S$$

$$\varepsilon_\varphi = \frac{\sigma_\varphi}{E} - \mu\frac{\sigma_z}{E} + \alpha T + B\int_0^t \left(\sigma_\varphi - \frac{1}{2}\sigma_z\right)dt + \frac{1}{3}S$$

(134)

where $B = C\Phi$.

The geometrical boundary conditions are

ε_z = const. over the cross section A; i.e. bending is restrained,

ε_φ = const. over the wall thickness h = R-r; i.e. tube is thin-walled.

In formulas these conditions can be written as

$$\varepsilon_z = \frac{1}{A} \int_A \varepsilon_z \, dA' = \overline{\overline{\varepsilon_z}} \tag{135}$$

$$\varepsilon_\varphi = \frac{1}{h} \int_h \varepsilon_\varphi \, d\varrho = \overline{\varepsilon_\varphi} \tag{136}$$

Note that two bars are standing for taking the mean over the whole cross section and one bar for taking the mean over the tube thickness.

The equilibrium in the axial and circumferential directions is described by

$$\int_A \sigma_z \, dA' = \overline{\overline{\sigma_z}} \, A = p_i \, r^2 \pi \tag{137}$$

and

$$\int_h \sigma_\varphi \, d\varrho = \overline{\sigma_\varphi} \, h = p_i \, r \tag{138}$$

Combination of Eqs. (134-136) yields

$$\frac{1}{E}(\sigma_z - \mu\sigma_\varphi) + \alpha T + \int_0^t [B(\sigma_z - \tfrac{1}{2}\sigma_\varphi) + \tfrac{1}{3}\dot{S}] \, dt = \frac{1}{E}\overline{\overline{(\sigma_z - \mu\sigma_\varphi)}} + \alpha\overline{\overline{T}} + \int_0^t \overline{\overline{[B(\sigma_z - \tfrac{1}{2}\sigma_\varphi) + \tfrac{1}{3}\dot{S}]}} \, dt \tag{139}$$

$$\frac{1}{E}(\sigma_\varphi - \mu\sigma_z) + \alpha T + \int_0^t [B(\sigma_\varphi - \tfrac{1}{2}\sigma_z) + \tfrac{1}{3}\dot{S}] \, dt = \frac{1}{E}\overline{(\sigma_\varphi - \mu\sigma_z)} + \alpha\overline{T} + \int_0^t \overline{[B(\sigma_\varphi - \tfrac{1}{2}\sigma_z) + \tfrac{1}{3}\dot{S}]} \, dt \tag{140}$$

Differentiation of Eqs. (139) and (140) with respect to time gives, considering that

$$\dot{T} = \overline{\dot{\overline{\sigma_\varphi}}} = \dot{\overline{\sigma_\varphi}} = \overline{\dot{\overline{\sigma_z}}} = 0 \tag{141}$$

$$\frac{1}{E}(\dot{\sigma}_z - \mu\dot{\sigma}_\varphi) + B(\sigma_z - \frac{1}{2}\sigma_\varphi) + \frac{1}{3}\dot{S} = \overline{\overline{B\sigma_z}} - \frac{1}{2}\overline{\overline{B\sigma_\varphi}} + \frac{1}{3}\overline{\overline{\dot{S}}} \qquad (142)$$

$$\frac{1}{E}(\dot{\sigma}_\varphi - \mu\dot{\sigma}_z) + B(\sigma_\varphi - \frac{1}{2}\sigma_z) + \frac{1}{3}\dot{S} = -\frac{1}{E}\mu\overline{\dot{\sigma}_z} + \overline{B\sigma_\varphi} - \frac{1}{2}\overline{B\sigma_z} + \frac{1}{3}\overline{\dot{S}}$$

$$(143)$$

From Eq. (142) integration over the tube thickness h results in

$$\frac{1}{E}\dot{\sigma}_z = \overline{\overline{B\sigma_z}} - \frac{1}{2}\overline{\overline{B\sigma_\varphi}} + \frac{1}{3}\overline{\overline{\dot{S}}} - \overline{B\sigma_z} + \frac{1}{2}\overline{B\sigma_\varphi} - \frac{1}{3}\overline{\dot{S}} \qquad (144)$$

Separation of Eqs. (142) and (143) yields the system

$$(145)$$

$$\frac{1}{E}\dot{\sigma}_z = \frac{1}{1-\mu^2}[(1-\frac{\mu}{2})(\mu\overline{B\sigma_\varphi} - B\sigma_z) + (\frac{1}{2}-\mu)(B\sigma_\varphi - \mu\overline{B\sigma_z})]$$
$$- \frac{1}{3(1-\mu)}(\dot{S} - \mu\overline{\dot{S}}) + \overline{\overline{B\sigma_z}} - \frac{1}{2}\overline{\overline{B\sigma_\varphi}} + \frac{1}{3}\overline{\overline{\dot{S}}}$$

$$\frac{1}{E}\dot{\sigma}_\varphi = \frac{1}{1-\mu^2}[(1-\frac{\mu}{2})(\overline{B\sigma_\varphi} - B\sigma_\varphi) - (\frac{1}{2}-\mu)(\overline{B\sigma_z} - B\sigma_z)] - \frac{1}{3(1-\mu)}(\dot{S} - \overline{\dot{S}}) \qquad (146)$$

These two differential equations were solved numerically step by step. The calculations were carried out for the state of constant operation with data listed in Table 1. The heat flux distribution described by Eq. (47) was assumed. The thermal computations yield a maximum temperature T_{max} = 520°C at φ = 0 and ϱ = R.

From Fig. 19 the complete history of circumferential stresses can be understood. Nearly immediately after the start of operation the stress state is given by the sum of thermoelastic stresses and stresses caused by internal pressure p_i. Theses stresses relax due to irradiation creep against a level given by the internal pressure. After swelling becomes noticeable compressive stresses are generated in high temperature regions and tensile stresses in low temperature regions because swelling at high temperatures is higher than swelling at low temperatures. For high doeses of neutron irradiation a stationary stress distribution results.

A similar behaviour can be observed for axial stresses represented in Fig. 20 for $\varphi = 0$. The compressive stresses near the plasma side become very high because of the completely prevented bending deformations. In a more realistic elastic-plastic analysis all compressive stresses in the outer region of the tube wall would be reduced due to plastic flow if the effective stress exceeded the temperature dependent yield stress. Also additional stress redistributions will affect the elastically calculated stress distributions. This effect will be small, since only in a layer of approximately 15% of the wall thickness and only near $\varphi = 0$ the effective stresses exceed the yield strength of SS 316 (20 % CW).

5.2 An analytical solution for the stationary stresses

The asymptotically reached state of stationary stresses can be calculated analytically. This state is characterized by

$$\dot{\sigma}_z = \dot{\sigma}_\varphi = \overline{\dot{\sigma}}_z = 0 \tag{147}$$

With this condition Eqs. (145) and (146) can be written in a simplified manner

$$B\,\sigma'_{\varphi_\infty} = \overline{B\,\sigma'_{\varphi_\infty}} + \tfrac{2}{3}\,\overline{S} - \tfrac{2}{3}\,\dot{S} \tag{148}$$

$$B\,\sigma'_{z_\infty} = \overline{B\,\sigma'_{z_\infty}} + \tfrac{2}{3}\,\overline{S} - \tfrac{2}{3}\,\dot{S} \tag{149}$$

$$B\,\sigma'_{z_\infty} = \overline{\overline{B\,\sigma'_{z_\infty}}} - \tfrac{1}{2}\,\overline{\overline{B\,\sigma'_{\varphi_\infty}}} + \tfrac{1}{3}\,\overline{\overline{S}} + \tfrac{1}{2}\,\overline{B\,\sigma'_{\varphi_\infty}} + \tfrac{1}{3}\,\overline{S} - \tfrac{2}{3}\,\dot{S} \tag{150}$$

subscript "∞" is standing for "dose $\rightarrow \infty$".
Taking into account the equilibrium conditions

$$\overline{\sigma'_{\varphi_\infty}} = P_i\,\frac{R}{h} \qquad\qquad \overline{\overline{\sigma'_{z_\infty}}} = P_i\,\frac{R}{2h} \tag{151}$$

one obtains the stationary stresses

$$\sigma_{\varphi_\infty} = \frac{pR + \frac{2}{3}\overline{\dot{S}/B} \cdot h}{B \cdot \overline{1/B} \cdot h} - \frac{2}{3}\dot{S}/B \tag{152}$$

and

$$\sigma_{z_\infty} = \frac{1}{3}\frac{\overline{\overline{\dot{S}/B}}}{B\,\overline{\overline{1/B}}} + \frac{1}{2}\frac{pR + \frac{2}{3}\overline{\dot{S}/B} \cdot h}{B\,\overline{1/B}\,h} - \frac{2}{3}\dot{S}/B \tag{153}$$

Because of the proportionalities, Eqs. (129) and (134),

$$\dot{S} = R(T)\,\phi \qquad B = C\,\phi$$

the quotients $\dot{S}/B$ become independent of the intensity of radiation, and it results

$$\sigma_{\varphi_\infty} = \frac{p_i R/h + \frac{2}{3C}\overline{R(T)}}{\phi \cdot \overline{1/\phi}} - \frac{2}{3C}R(T) \tag{154}$$

$$\sigma_{z_\infty} = \frac{1}{3C}\frac{\overline{\overline{R(T)}}}{\phi\,\overline{\overline{1/\phi}}} + \frac{1}{2}\frac{p_i R/h + \frac{2}{3C}\overline{R(T)}}{\phi \cdot \overline{1/\phi}} - \frac{2}{3C}R(T) \tag{155}$$

Especially for a <u>thin-walled tube</u> we obtain

$$\sigma_{\varphi_\infty} \cong p_i\frac{R}{h} + \frac{2}{3C}[\overline{R(T)} - R(T)] \tag{156}$$

$$\sigma_{z_\infty} \cong p_i\frac{R}{2h} + \frac{1}{3C}[\overline{\overline{R(T)}} + \overline{R(T)} - 2R(T)] \tag{157}$$

5.3 Influence of sputtering

If sputtering is taken into account the wall thickness can
be written approximately as

$$h \approx h_0 - \text{const.} (\phi t)$$ (158)

where h_0 is standing for the thickness at the beginning of the
operation. The constant in Eq. (158) has been chosen so that
$dh/dt \approx 2$ mm/year. Solution of Eqs. (145) and (146) with this
variable wall thickness gives the stress development represen-
ted in Fig. 21 for $\varphi = 0$. The curves indicated by dotted-dashed
lines are the extremal stresses without sputtering as shown in
Fig. 19. For short times, i.e. low dose, there is an identical
stress state. The reduction of wall thickness at higher dose
yields a lower gradient of temperature in the wall and, con-
sequently lower thermal stresses.

As there is a constant internal pressure the vanishing wall
thickness gives rise to high tensile stresses. Failure occurs
if the wall thickness tends to zero, and the stresses become
infinite. Since there is a great uncertainty in knowledge of
sputter rates this effect shall not be considered in the fol-
lowing sections.

5.4 Cyclic stresses in the tube wall

In most fusion reactors the plasma is heated by direct-cur-
rent, with the plasma acting as a secondary winding of a
transformer. The magnetic field varies with constant slope
creating a constant current in the plasma. Before the mag-
netic field reaches saturation reactor operation has to be
interrupted. By this reactor operation becomes cyclic.

As a consequence of these cycles the thermal stresses change
periodically. If the burn-off times are long enough, the tem-
perature in the whole tube wall will become nearly equal to

the temperature T_o of the coolant medium. Due to this tempe-
rature changes $\Delta T = T - T_o$ cyclic thermoelastic stresses
occur. For shorter interruptions the assumption of complete
temperature balance in the wall becomes a worst case assump-
tion with respect to crack growth behaviour.

Figure 22 shows the cyclic stresses for the plasma side and
the coolant side (note that burn time and refuelling time are
not on the correct scale!). The maximum values are named σ_{max}
the minimum values σ_{min}. The inner surface undergoes maximum
stress during burning time, the inner surface during refuelling
time. The occurrence of high tensile peaks at the plasma side
during refuelling time is of high interest. Those cyclic stes-
ses give rise to the growth of pre-existing cracks.

6. Calculation of stress intensity factors

Cyclic stresses are responsible for crack growth. In welded con-
structions pre-existing cracks cannot be excluded because de-
fects can only be detected above a minimum size. The fracture
mechanical loading quantity characterizing the stress state
at the crack tip is the stress-intensity factor K. If a is the
depth of a crack (Fig. 23) and $\sigma(x)$ the stress distribution
in the uncracked wall, the stress intensity factor for two-
dimensional crack problems is given by the basic equation

$$K(a) = \int_0^a \sigma(x) \, H(x,a) \, dx \tag{159}$$

where $H(x,a)$ is the so-called weight function. In this report
only continuous cracks (i.e. cracks are as long as the tube)
have been taken into account, because they are the most serious
one. Lifetime calculated with such cracks obviously become
conservative. This means that more realistic cracks with the
same crack depth, i.e. semi-elliptical cracks, will fail later.

In a normalized representation Eq. (159) can be expressed as

$$K = \sqrt{R-r} \int_0^\alpha \sigma(\xi) \, h(\xi, \alpha) \, d\xi \tag{160}$$

$$\xi = \frac{x}{R-r} \quad ; \quad \alpha = \frac{a}{R-r}$$

Cracks situated at the inner surface can be treated by application of the weight function given by Labbens [27, 28]

$$h(\xi, \alpha) = \sqrt{\frac{2}{\pi \alpha}} \; \frac{\gamma + \xi/\alpha}{\gamma + \alpha} \; \frac{m(\xi/\alpha, \alpha)}{\sqrt{1 - \xi/\alpha}} \tag{161}$$

where $\gamma = \dfrac{r}{R-r}$

$m(\xi/\alpha, \alpha)$ can be expressed by polynomials

$$m(\xi/\alpha, \alpha) = 1 + \sum_{i=1}^{4} b_i(\alpha) \left(1 - \frac{\xi}{\alpha}\right)^i \tag{162}$$

whereby

$$b_1(\alpha) = \sum_{i=0}^{4} c_i \, \alpha^i \qquad b_2(\alpha) = \sum_{i=0}^{4} d_i \, \alpha^i$$

$$b_3(\alpha) = \sum_{i=0}^{4} e_i \, \alpha^i \qquad b_4(\alpha) = \sum_{i=0}^{4} f_i \, \alpha^i \tag{163}$$

The coefficients of the polynomials are known for $\gamma = 5$ and $\gamma = 10$. They are listed in Table 2. Unfortunately, the weight function of Labbens is only given for inner surface cracks and only for discrete values of the ratio (wall thickness/ inner radius). In this investigation $\gamma = 10$ was applied.

Since no weight function for continuous cracks situated at the outer surface is available the crack problem has to be simplified. A simple approximation is possible by applica-

tion of a so-called "edge-crack", i.e. a continuous crack in a plane sheet of thickness w = R-r. For outer surface cracks the inequality yields

$$K_{\text{inner surface}} < K_{\text{outer surface}} < K_{\text{edge crack}} \qquad (164)$$

(same a,σ in all three cases)

so that by application of $K_{\text{edge crack}}$ a worst case approximation results.

The weight function of the edge crack given by Bückner [29] is

$$h(\xi,\alpha) = \sqrt{\frac{2}{\pi\alpha}} \; \frac{1}{\sqrt{1-\xi/\alpha}} \; [1 + m_1(1-\xi/\alpha) + m_2(1-\xi/\alpha)^2] \qquad (165)$$

$$m_1 = c_0 + c_1\alpha^2 + c_2\alpha^6$$

$$m_2 = d_0 + d_1\alpha^2 + d_2\alpha^6$$

$$c_0 = 0,6147 \qquad\qquad d_0 = 0,2502$$

$$c_1 = 17,1844 \qquad\qquad d_1 = 3,2889$$

$$c_2 = 8,7822 \qquad\qquad d_2 = 70,0444$$

Equation (165) is valid in the range $0 < \alpha < 0,5$.
The stress intensity factors for continuous operation are plotted in Fig. 24 for inner surface cracks of different sizes situated at different locations φ. On account of Eq. (160) the stress intensity factor K changes with respect to the dose in the same manner as σ.

K decreases with increasing φ as a result of lower temperature gradients. Figure 25 shows a similar behaviour for outer surface cracks.

Cyclic operation of a fusion reactor causes cyclic thermal stresses in the range $\Delta\sigma(\varrho,\varphi)$. Due to these stresses a cyclic stress intensity factor ΔK results from Eq. (160). Figure 26 shows ΔK as a function of crack size a and location φ. The highest cyclic stresses location is at $\varphi = 0$ as has been expected. The ΔK-values for inner surface cracks are but slightly higher than ΔK-values for outer surface cracks. This is no discrepancy with respect to Eq. (164) because inner and outer cracks are not influenced by the same stresses. With the inequality (164) also taken into account one can conclude that deviations caused by the "edge-crack assumption" are negligible. Superposition of K-values during constant operation and ΔK-values due to thermal cycling gives the complete K-behaviour. In Fig. 27 K_{max}, ΔK and the minimum values

$$K_{min} = K_{max} - \Delta K \qquad (166)$$

are represented.

7. Crack growth behaviour

The propagation of cracks in cyclically loaded structures is mainly a consequence of plastic deformations at the crack tip. These deformations and hence the crack growth rate are controlled by ΔK. Other crack growth mechanisms caused by static load in a corrosive environment shall be excluded. For ΔK-controlled crack growth numerous relationships were developed since the early 1960's. One of the best-known is the Paris-equation [30].

$$\frac{da}{dN} = C(\Delta K)^n \qquad (167)$$

Where da/dN is the crack extension due to one cycle, C and n are constants depending on the material and environment.

By measurements a minimum ΔK-value was found below which no crack growth occurs. This value is called the threshold ΔK_{th}. Taking into account an acceleration of crack growth rate near the critical stress intensity factor K_{Ic} a modified Forman equation proposed by Speidel [34] seems to be most effectively adopted. It reads

$$\frac{da}{dN} = \frac{C_1 \, \lambda^m \, [\, f \, \Delta K - \Delta K_0 \,]^n}{K_{Ic} - \lambda \, f \, \Delta K} \tag{168}$$

where $\lambda = \dfrac{1}{1 - R}$

and $f = E(T_1)/E(T)$ is a correction factor to model the temperature effect caused by the temperature dependent Young's modulus. T_1 is standing for room temperature.
For R two cases have to be distinguished:

1) Crack of the coolant side (inner surface)

K^{th} is the stress intensity factor for thermal stresses only and K_{on} notes the stress intensity factor for constant operation ("plasma on"), then

$$R = \frac{K_{min}}{K_{max}} = \frac{K_{on} - K^{th}}{K_{on}}$$

2) Crack at the plasma side (outer surface)

Here $K^{th} < 0$

and therefore

$$R = \frac{K_{min}}{K_{max}} = \frac{K_{on}}{K_{on} - K^{th}}$$

The material constants for stainless steels are taken from Watson [6] for room temperature and air as the environment

$$C_1 = 3.122 \cdot 10^{-9} \quad m/cycle$$
$$n = 2.95$$
$$K_{Ic} = 150 \, MPa \, \sqrt{m}$$

$$m = \begin{cases} 1 - 0.31 R - 1.23 R^2 & R > 0 \\ 1.88 & R < 0 \end{cases} \tag{169}$$

$$\Delta K_0 = \begin{cases} 5.4 \, (1 - 0.9 R) & \\ 5.4 \, (1 - 0.2 R) & \end{cases} MPa \sqrt{m} \quad \begin{array}{l} R > 0 \\ R < 0 \end{array}$$

The tube investigated fails when K_{max} reaches the critical stress intensity factor K_{Ic}. Because of irradiation embrittlement this K_{Ic} is not a constant, but decreases with the neutron dose. In the literature different correlations are reported with K_{Ic} always decreasing as an exponential equation. Differences can be stated in the occurrence of an asymptotically reached limit value. Our calculations were carried out with an equation [6]

$$(170)$$

$$K_{Ic} = 115 \exp(-0.25\,\phi t) + 35 \exp(-0.0134\,\phi t)$$

that does not exhibit a limit value.

The crack growth behaviour is represented in Fig. 28 - 31. In these diagrams the fluence has been chosen as 22 dpa/year. For inner surface cracks shown in Fig. 28 the maximum stress intensity factor K_{max} decreases for short operation times because the stresses relax in this region. At higher dose this effect becomes overcompensated by increasing crack depth. Failure occurs when the rapidly increasing curve crosses the K_{Ic}-curve. As expected, small cracks lead to longer lifetimes. From Fig. 29 it can be seen that not only cracks situated at the inner surface will cause failure but also cracks at the outer surface where mostly compressive stresses are suspected. From variations of the angle φ in Fig. 30 and 31 one concludes a most serious location for fatigue failure, namely at $\varphi = 0$, so that future investigations should be restricted to that place.

An increase of lifetime for reduced tube wall thickness can be stated from Fig. 35 because temperature gradients are reduced too.

8. Summary

The methodology of lifetime calculations for plasma affected first wall components has been treated in case of a pressurized blanket tube. The analysis was carried out in the following steps:

- Calculation of the instationary temperature distribution for an asymmetrically heated tube with different chosen heat flux distributions.

- Computation of thermoelastic stresses in the tube wall.

- Influence of volumetric heat and noncircular tube cross sections were taken into account.

- The influence of irradiation creep and swelling on the development of stress distributions were analyzed.

- Cyclic operation gives rise for cyclic thermal stresses and pre-existing cracks in the tube wall can grow as fatigue cracks.
  In a conservative analysis such cracks were assumed as continuous cracks (i.e. cracks are as long as the tube).

- Caused by the high thermal loading ($\sim$ 40 W/cm^2) and the conservative crack assumption only relative short lifetimes were obtained.

In a further investigation it is planned to consider more realistic cracks as semi-elliptical surface cracks and also crack initiation. In case of water cooled tubes crack growth of inner surface cracks will be calculated with data given in [32].

Also a comparison of different candidate materials will be executed, employing the material data of a martensitic steel.
The treatment of more complex structures will be taken into account starting with the actual NET-first wall design.

9. References

/1/ R.F. Mattas, D.L. Smith, "Model for life-limiting properties of fusion reactor structural materials," Nuclear Technology, 38 (1978), pp. 186-198

/2/ W. Daenner, J. Raeder, "FWLTB - A computer program for predicting the lifetime of a fusion reactor first wall," Transact. of the 5th International Conference on Struct. Mech. in React. Technology, Berlin, Aug. 13-17, 1979, paper N 2.3/2

/3/ S.D. Harkness, B. Cramer, "A review of lifetime analysis for tokamaks," Journ. of Nuclear Materials 85 a. 86 (1979) pp. 135-145

/4/ W. Daenner, "Results of strategic calculations for optimizing the first wall life in a tokamak fusion reactor," Transact. 6th Intern. Conf. on Struct. Mech. in Reactor Techn., Paris, Aug. 1981, Paper N 4/1

/5/ R.E. Watson, R.R. Peterson, W.G. Wolfer, "The effect of irradiation creep, swelling, wall erosion and embrittlement on the fatigue life of a tokamak first wall," 2nd Topical Meeting on Fusion Reactor Materials, 9-12 August 1981, Seattle WA

/6/ R.D. Watson, "The impact of inelastic deformation, radiation effects, and fatigue damage on fusion reactor first wall lifetime," Thesis, University of Wisconsin, 1981, UWFDM-460

/7/ A.M. Hassanein, "Thermal effects and erosion rates resulting from intense deposition of energy in fusion reactor first walls," Thesis, University of Wisconsin, 1982, UWFDM-465

/8/   R.F. Mattas, "Fusion component lifetime analysis," Ar-
      gonne National Laboratory-Report: ANL/FPP/TM-160

/9/   W. Daenner, "Lifetime considerations for the first wall
      of a demo reactor," Fusion Technology 1982, Vol. 2,
      pp. 857-862

/10/ R.W. Watson, R.R. Peterson, W.G. Wolfer, "Lifetime ana-
      lysis of fusion reactor first wall components," Trans-
      actions of the ASME, Journ. of Pressure Vessel Techno-
      logy, 105 (1983), pp. 144-152

/11/ W. Daenner, "FWLTB - A computer program for estimating
      the first wall lifetime in a fusion reactor: A status
      report," Res. Mechanica, 6 (1983) 183-191

/12/ A.O. Adegbulugbe, "Comparison of lifetime calculation for
      fusion reactor first walls based on two creep-fatigue de-
      sign criteria," Nuclear Engineering and Design/Fusion
      1 (1984) 301-305

/13/ A.M. Hassanein, G.L. Kulcinski, W.G. Wolfer, "Surface
      melting and evaporation during disruptions in magnetic
      fusion reactors," Nuclear Engineering and Design/Fusion
      1 (1984), 307-324

/14/ -   , "TASKA-M, a low cost, near term tandem mirror
      device for fusion technology testing," Karlsruhe (1984)
      KfK 3680

/15/ H.S. Carslaw, J.C. Jaeger, "Conduction of heat in solids,"
      Oxford University Press, 1959

/16/ A.G. Holms, "A biharmonic relaxation method for calcu-
      lating thermal stress in cooled irregular cylinders,"
      NACA-TN-2434, 1951

/17/ C.F. Kettleborough, "Non-axial-symmetric thermal stres-
      ses in circular discs or cylinders," Int. Journ. for
      Num. Methods in Engineering, 3, (1971) pp. 53 - 61

/18/ J.M. Chern, D.H. Pai, "Inelastic analysis of a straight
      tube under combined bending, pressure and thermal loads,"
      J. of Pressure Vessel Technology, 97 (1975) pp. 155-162

/19/ G.D. Gupta, M.S.M. Rao, T.V. Narayanan, A.C. Gangadharan,
      "Thermoelastic analysis of nonaxisymmetrically heated
      thick cylindrical shells," J. of Pressure Vessel Techno-
      logy, 100 (1978) pp. 107-111

/20/ Jahnke-Emde-Lösch, "Tables of higher functions," B.G.
      Teubner Verlagsgesellschaft, Stuttgart, 1960

/21/ E. Melan, H. Parkus, "Wärmespannungen infolge stationärer
      Temperaturfelder," Springerverlag, Vienna, 1953

/22/ W. Gröbner, N. Hofreiter, "Integraltafeln" I, 5. ed.,
      Vienna, 1975   (cf. No. 331/7a)

/23/ P.T. Heald, M.V. Speight; Philos. Mag., 1974, 29, 1075

/24/ W.G. Wolfer, M. Ashkin; J. Appl. Phys., 1975, 46, 547

/25/ K. Ehrlich, "Irradiation creep and interrelation with
      swelling in austenitic stainless steels," Journ. of Nucl.
      Materials 100 (1981) 149-166

/26/ W. Schneider, K. Herschbach, K. Ehrlich, "Interdependence
      of In-pile Creep and Void Swelling in Ti- and Nb-stabili-
      zed Stainless Steels," ASTM STP 782 (1982) 30-42

/27/ R. Labbens, A. Pellessier-Tanon, J. Heliot, "Practical
      method for calculating stress intensity factors through
      weight functions," Mechanics of Crack Growth, ASTM-STP 590,
      1976, 368-384

/28/ D.O. Harris, E.Y. Lim, "Stress intensity factors for complete circumferential interior surface cracks in hollow cylinders," Proceeding of the 13th National Symposium on Fracture Mechanics, ASTM-STP 743, 1981, 375-386

/29/ H.F. Bueckner, "Field singularities and related integral expressions," Mechanics of Fracture 1, - Methods of Analysis and Solution of Crack Problems, Nordhoff Int. 1973

/30/ P.C. Paris, F. Erdogan, "A critical analysis of crack propagation laws," Journ. of Basic Engineering, 85 (1963), 528-534

/31/ M.O. Speidel, "Fatigue crack growth at high temperatures," Proc. of the Symposium on high-temperature materials in gas turbines, Switzerland, 1974, 207-251

/32/ - ; "ASME Boiler and Pressure Vessel Code," Sec. XI 1980 ed.

Table 1

Dimensions (size) and working conditions

Surface heat flux	$\dot{Q}$	= 40 W/cm^2
Outer radius	R	= 10 cm
Ratio of radii	R/r	= 1.1
Temperature of coolant medium	T_o	= 350°C
Internal pressure	P_i	= 100 bar
Burn time		19 minutes
Refuelling time		1 minute
Material		SS 316 (20% CW)

Table 2

Coefficients for weight function of Labbens

	= 5	= 10		= 5	= 10
c_0	1.52534	1.99729	e_0	2.38462	19.72683
c_1	-7.64696	-15.03191	e_1	-17.05922	-267.73618
c_2	43.47251	78.59787	e_2	60.78644	1156.07329
c_3	-53.85642	-110.27903	e_3	-64.32954	-1895.15242
c_4	28.87155	66.66854	e_4	12.96156	1024.52402
d_0	-2.87331	-11.24627	f_0	-0.79108	-10.72898
d_1	30.99174	153.95536	f_1	3.06121	149.79271
d_2	-126.08387	-671.65647	f_2	-9.39198	-617.77169
d_3	209.31849	1121.96619	f_3	-3.99661	999.26996
d_4	-106.99770	-602.83976	f_4	14.22188	-533.71745
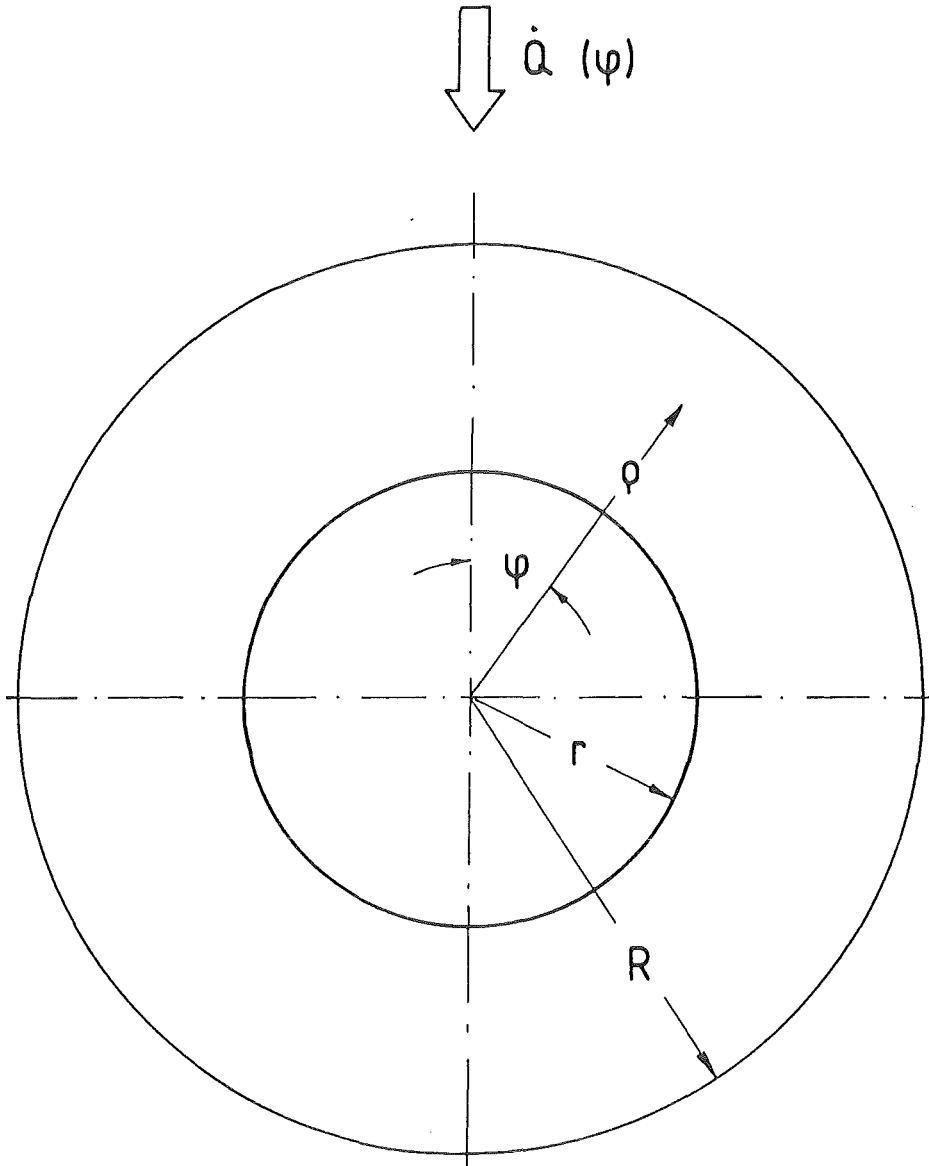
Figure 1:   Geometric units of the tube wall
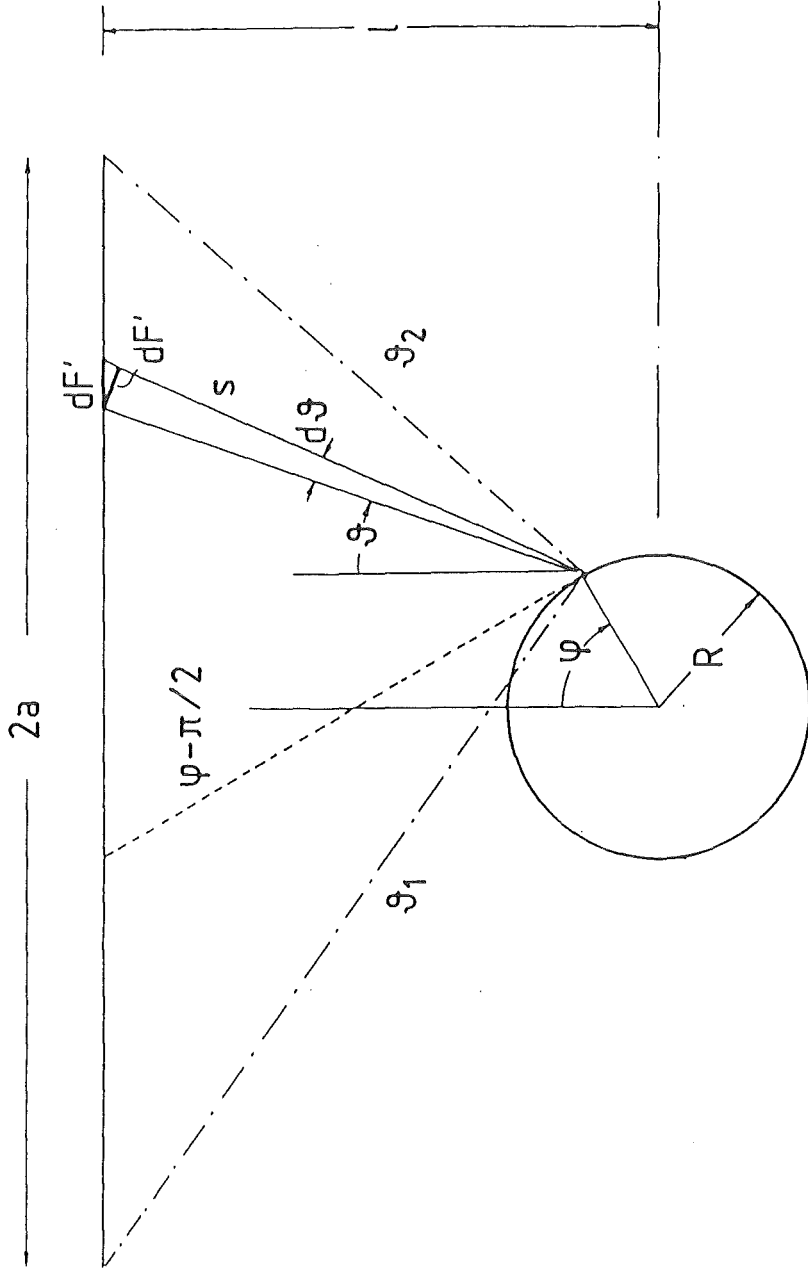
Figure 2:   Tube in front of a heat radiating endless strip
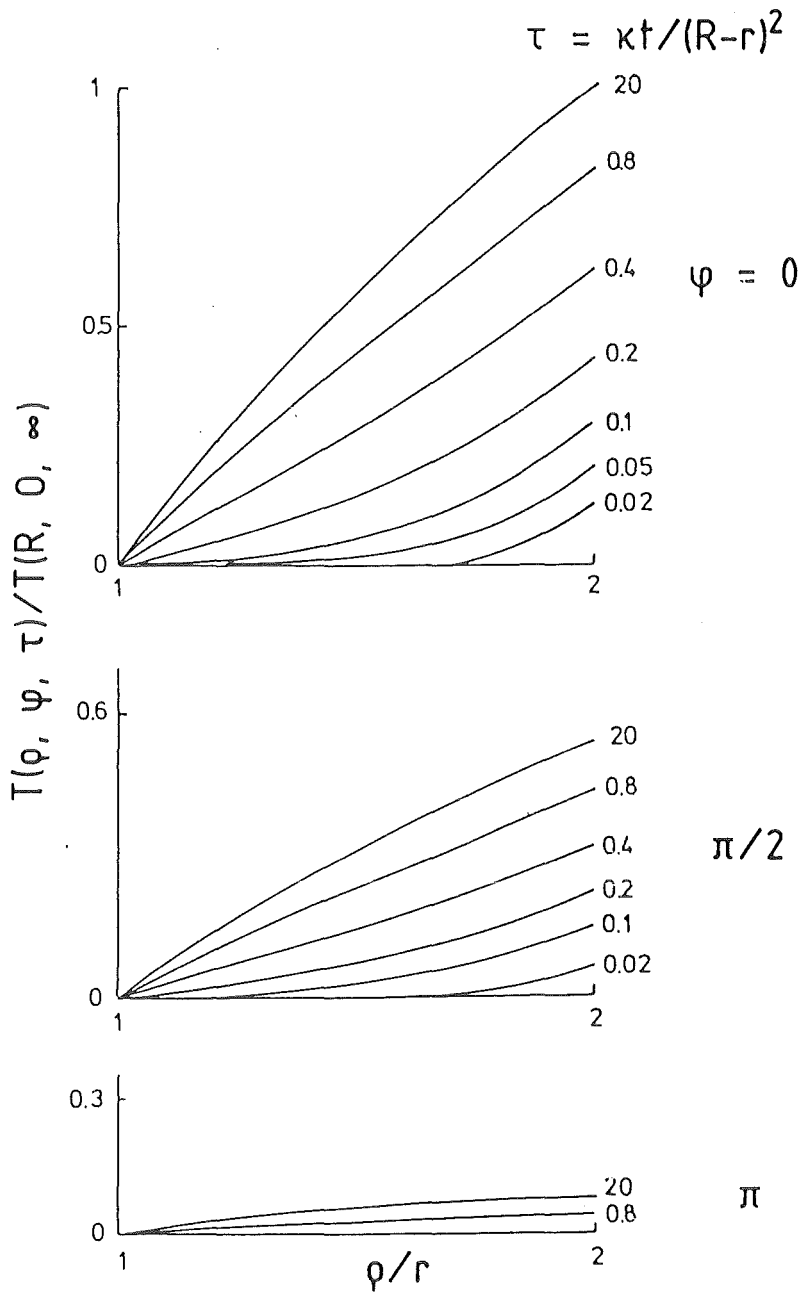
Figure 3:   Time dependent temperature distribution in a tube in front of a heat radiating half-space
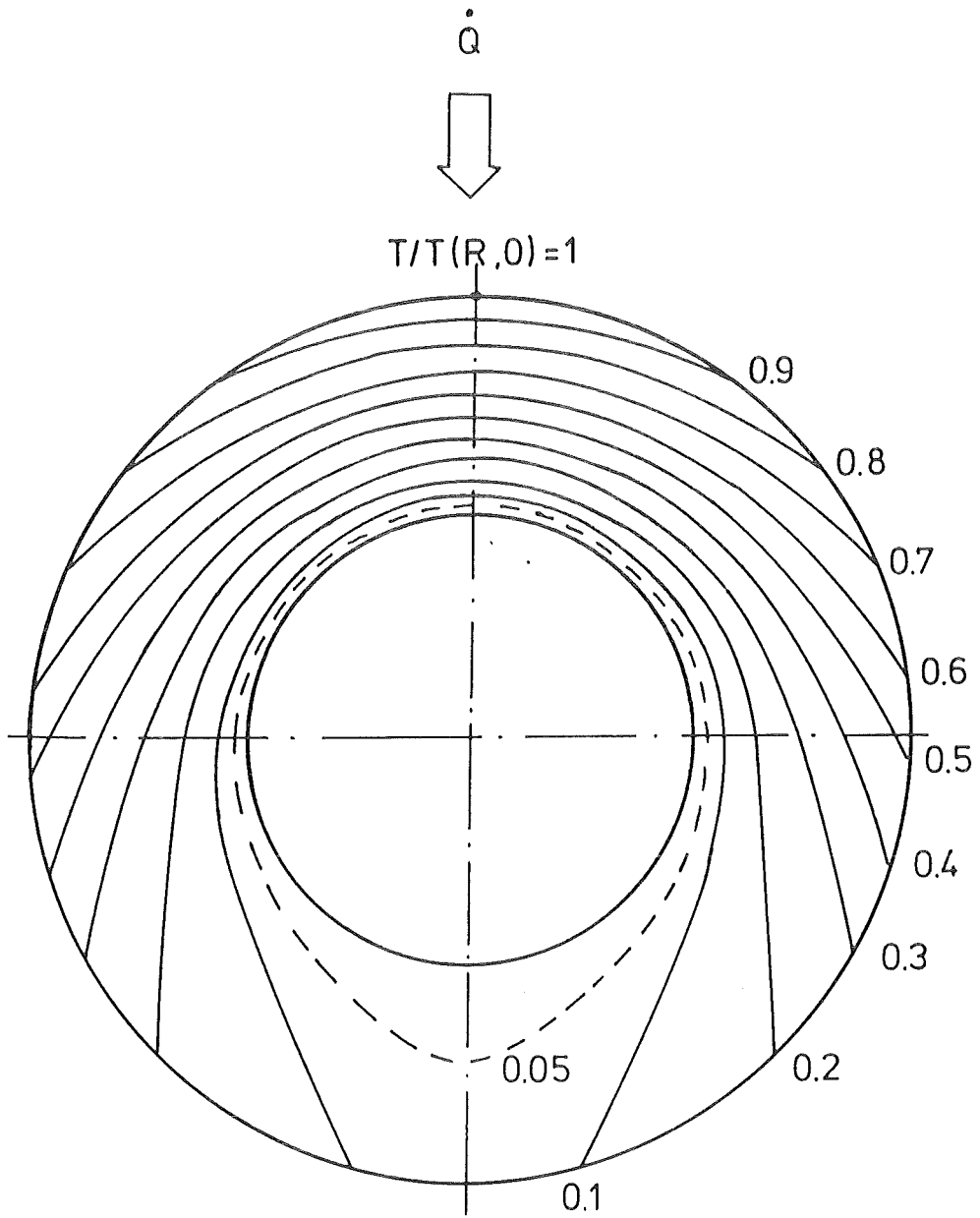
Figure 4 :   Isotherms in case of a heat radiating half-space
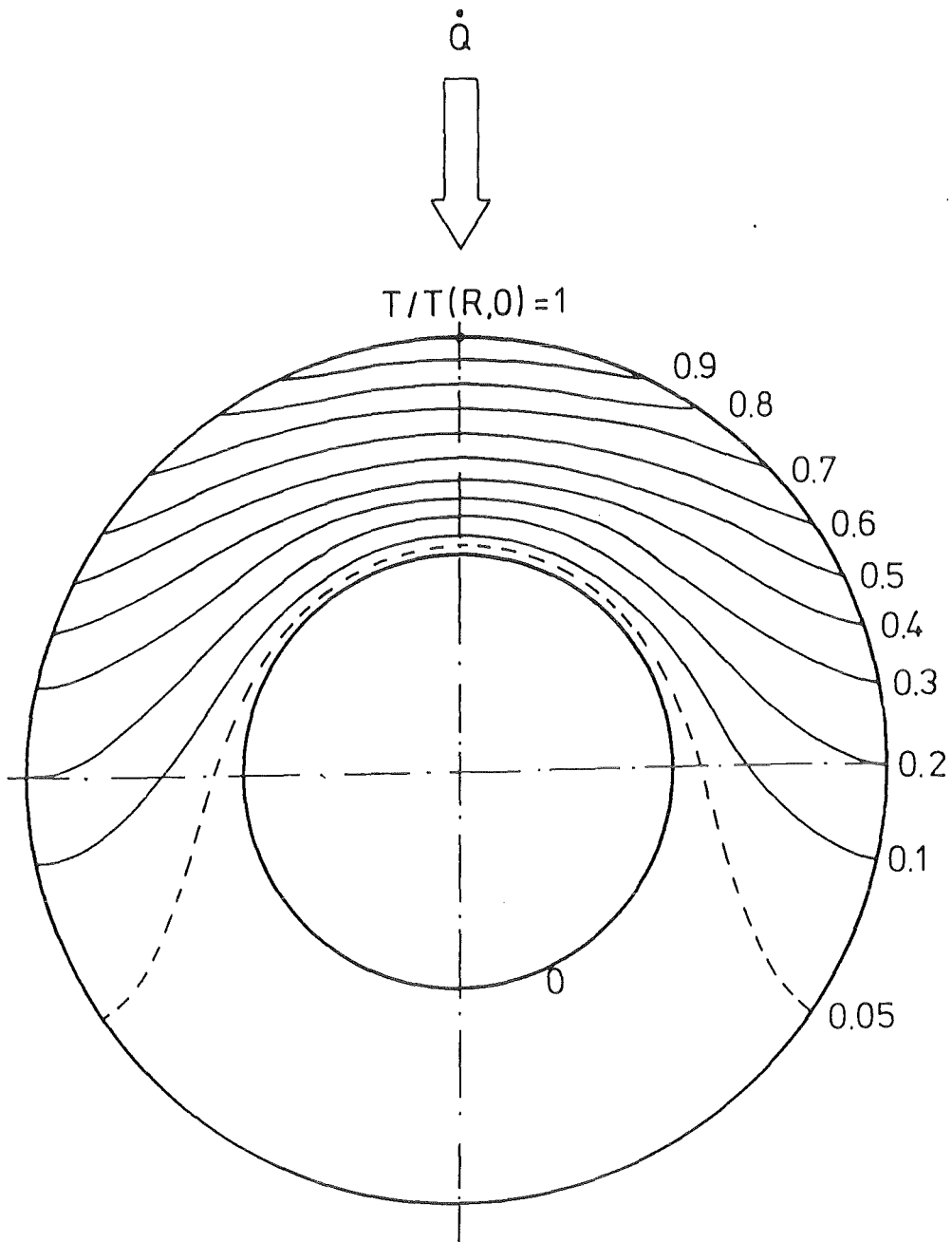
Figure 5:   Isotherms in case of a radiation source at an infinite
distance from the tube
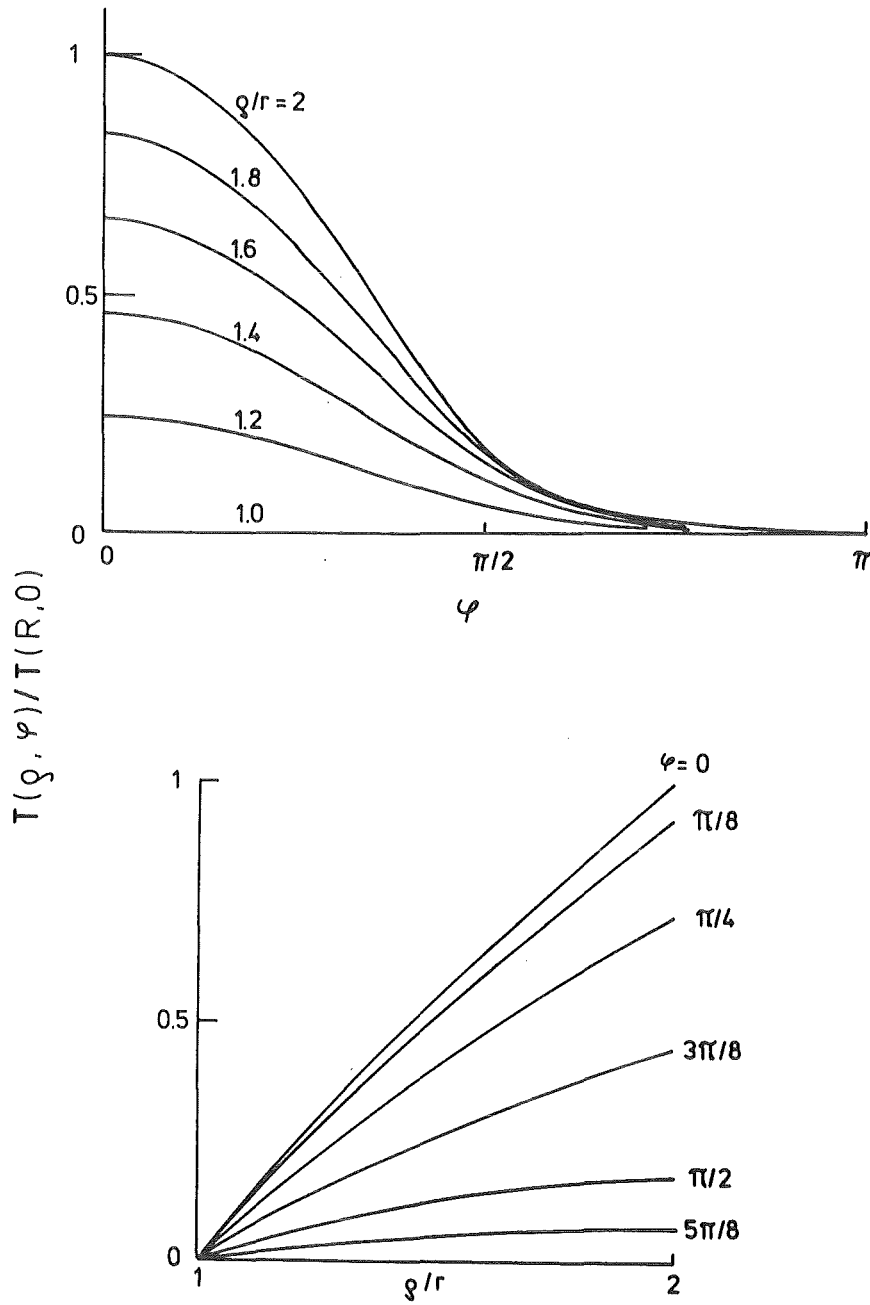
Figure 6:   Stationary temperature distribution referring to Figure 5
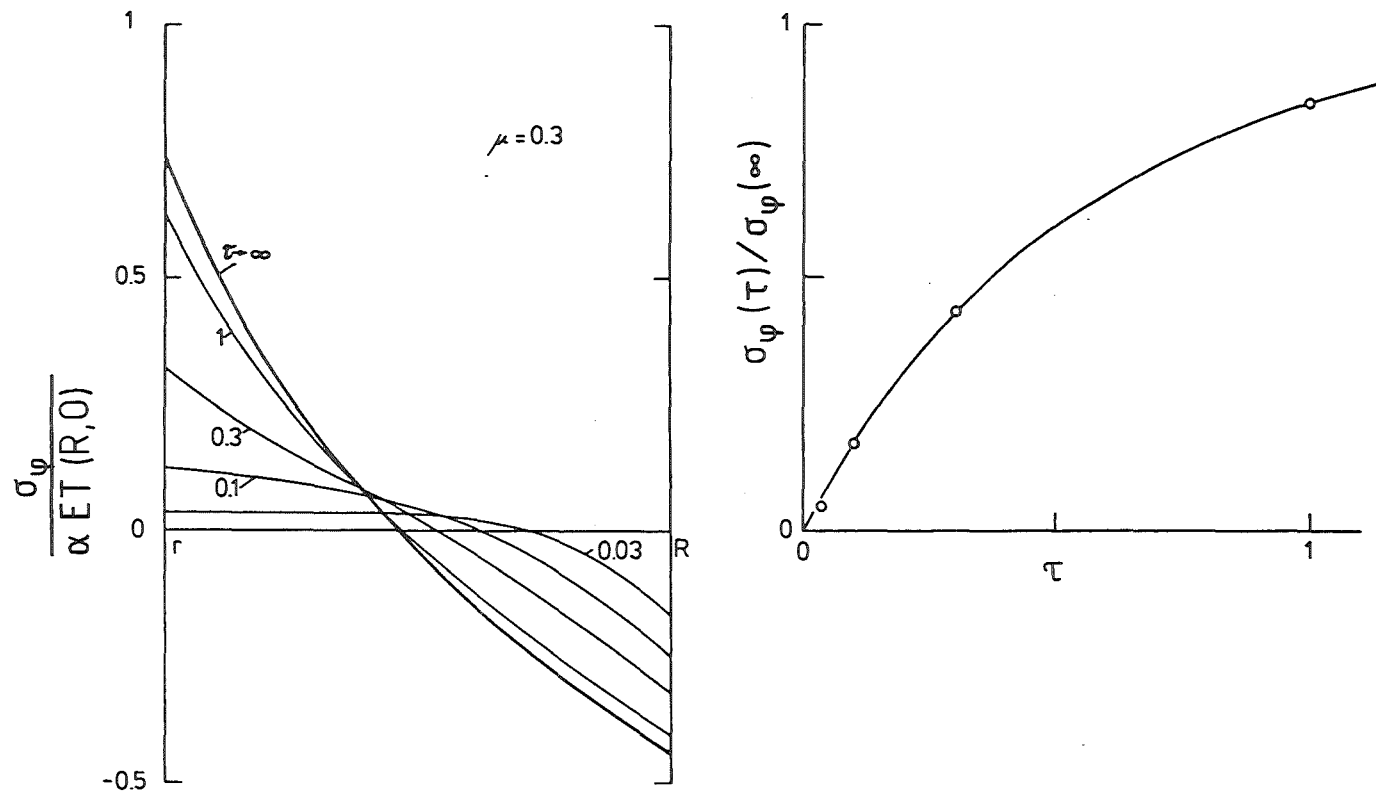
Figure 7: Instationary circumferential stresses in a tube in front of a heat radiating half-space
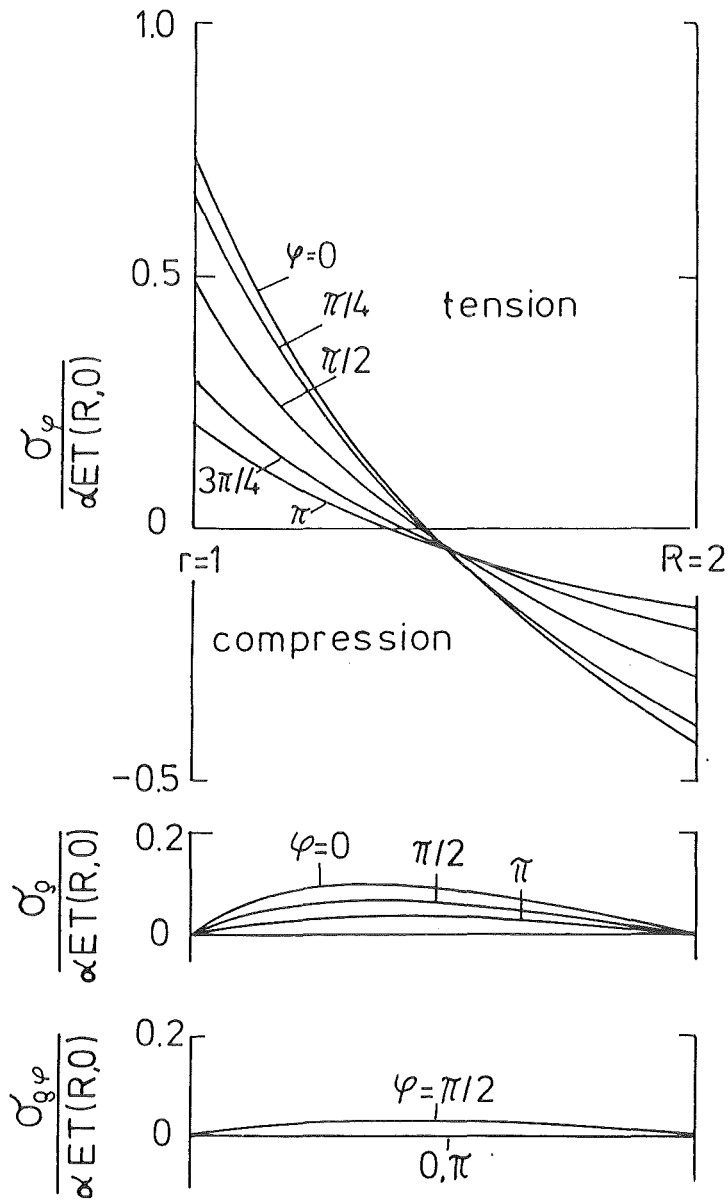
Figure 8 :   Stationary stress distributions for different values
of φ
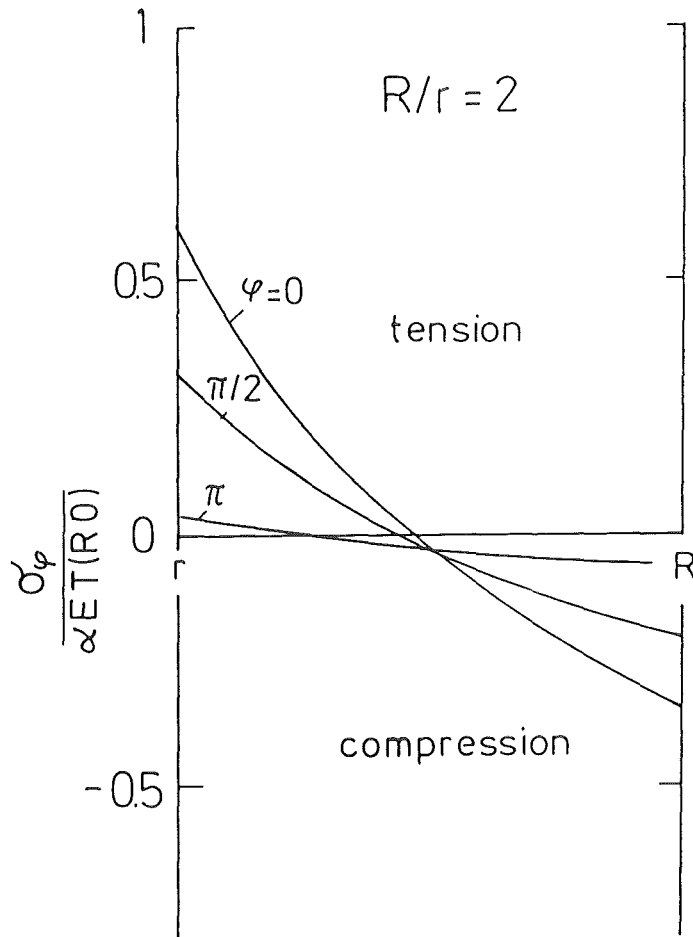
Figure 9:   Circumferential stresses in a tube heated by a radiation source placed at an infinite distance.
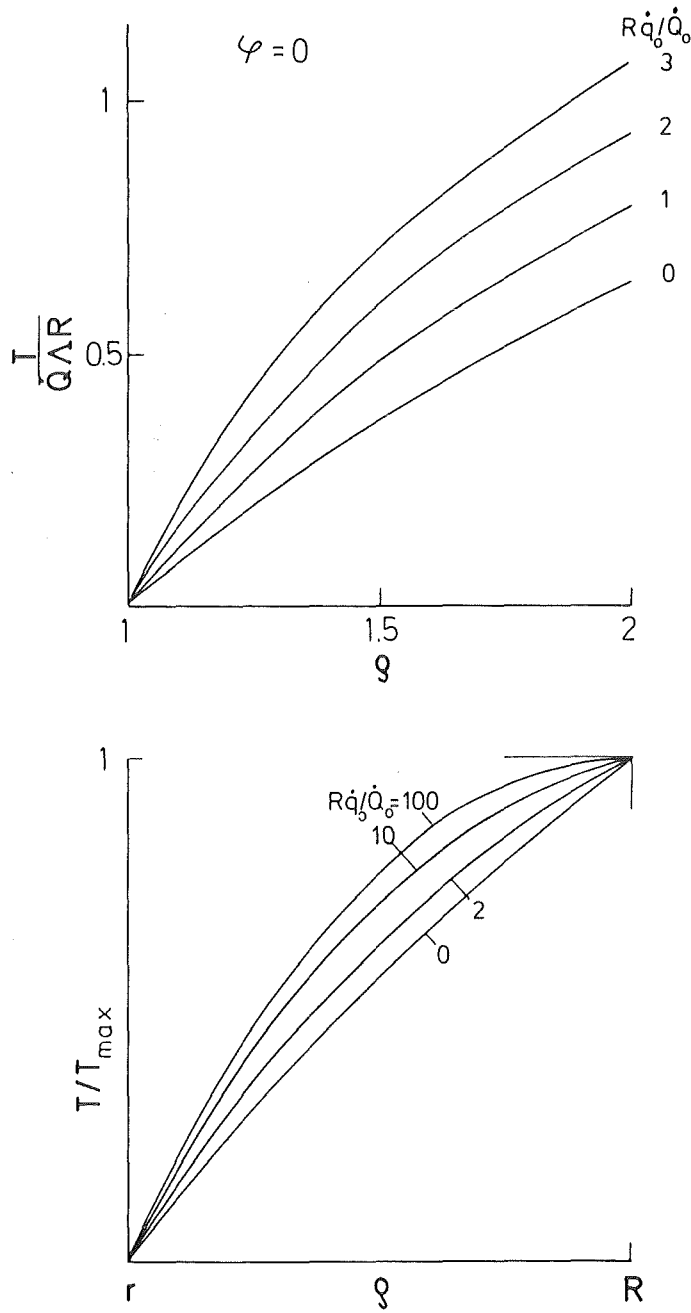
Figure 10   Influence of volumetric heating on the stationary
temperature distribution
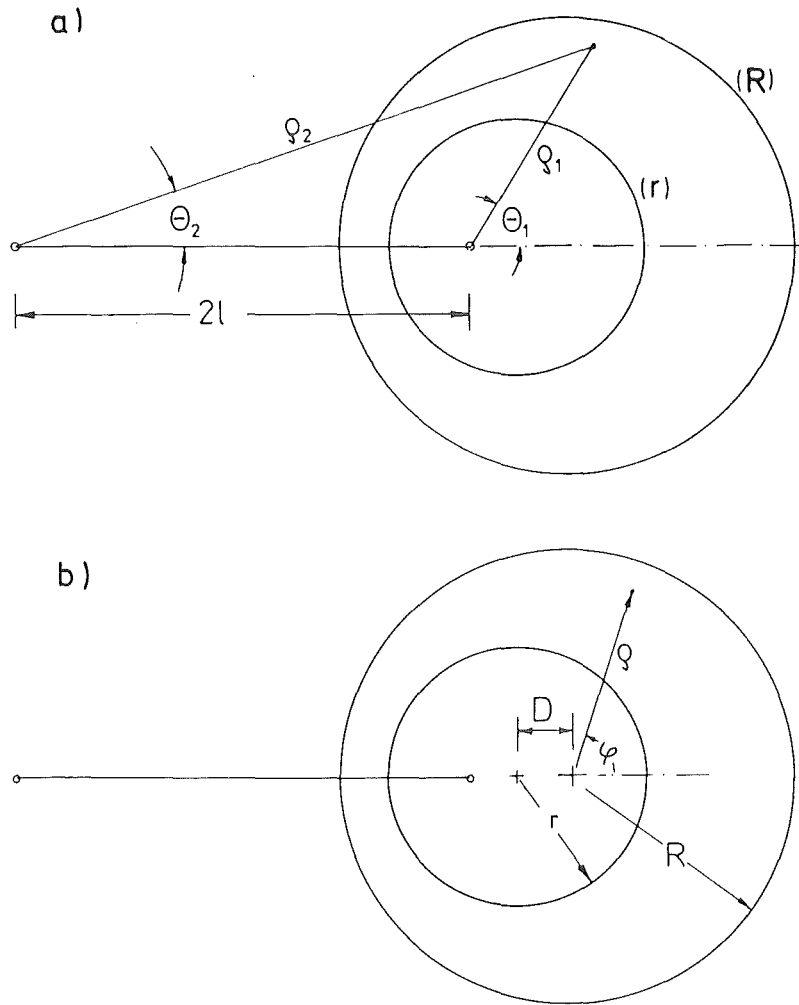
Figure 11   Geometrical units of an eccentric tube wall
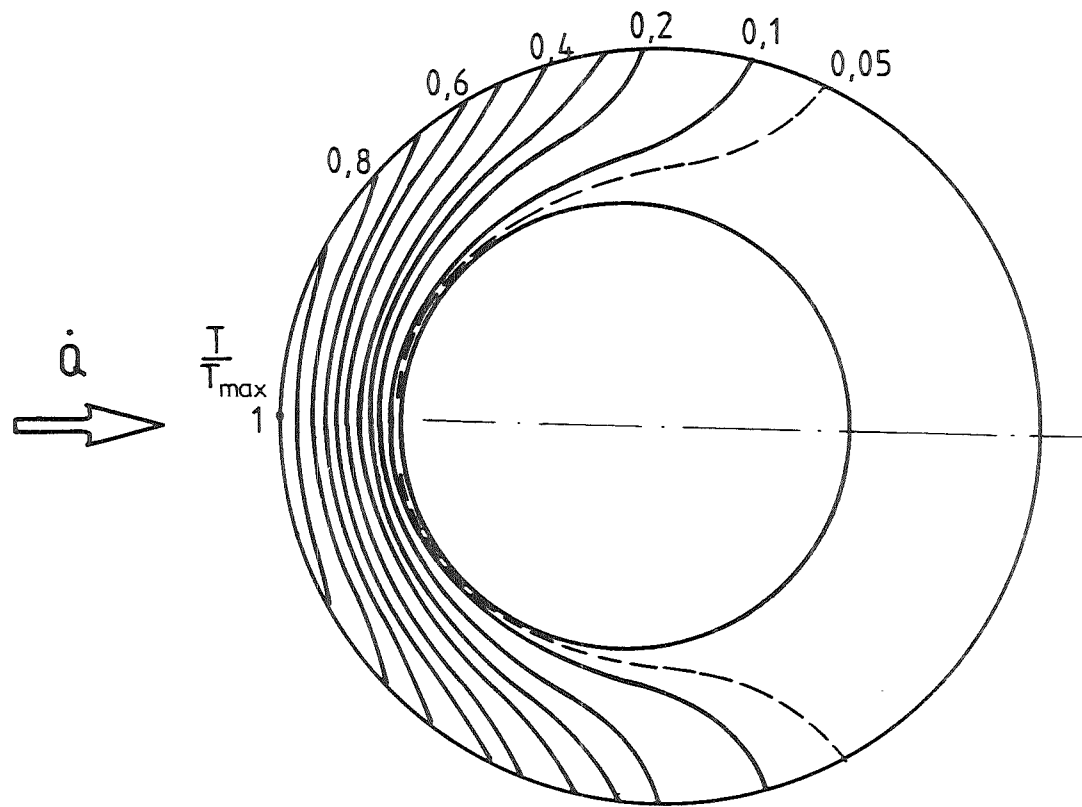
Figure 12   Isotherms of stationary temperature for an eccentric tube
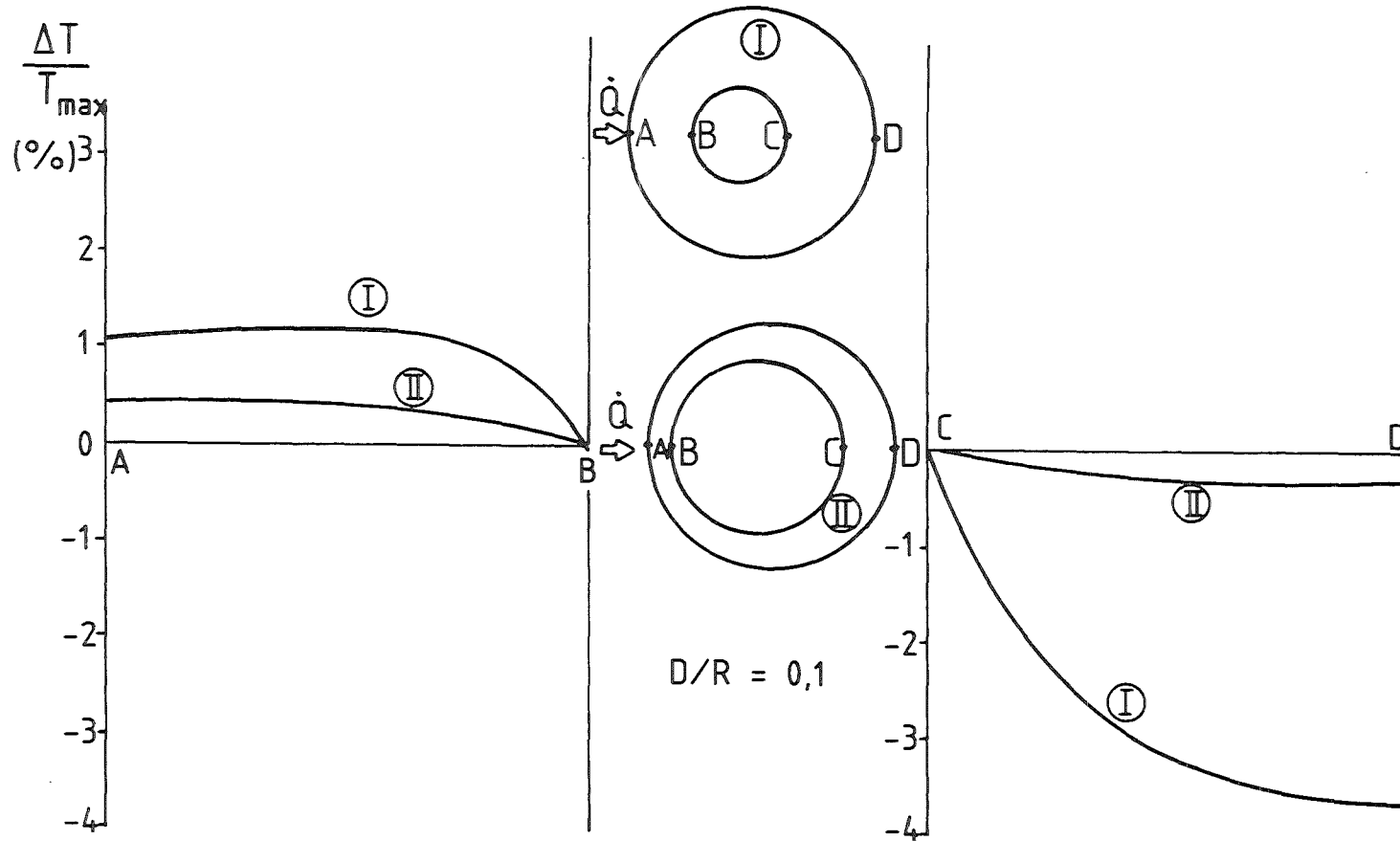
Figure 13   Deviations between exact and approximate stationary
            temperature distributions for different shaped eccentric tubes
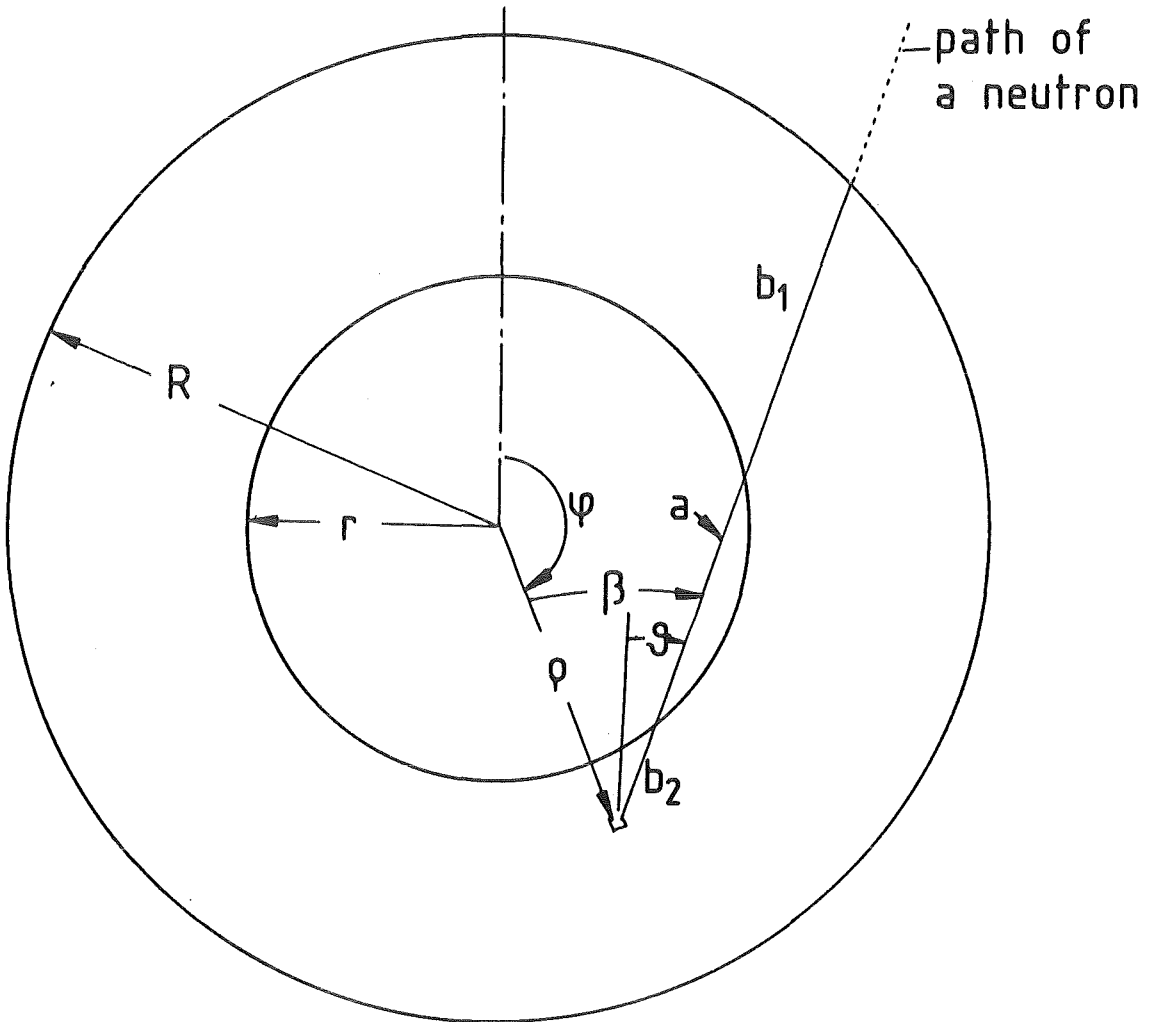
Figure 14   Geometric quantities for calculation of neutron
intensity in the tube wall

$$\alpha_2 \longrightarrow 0$$
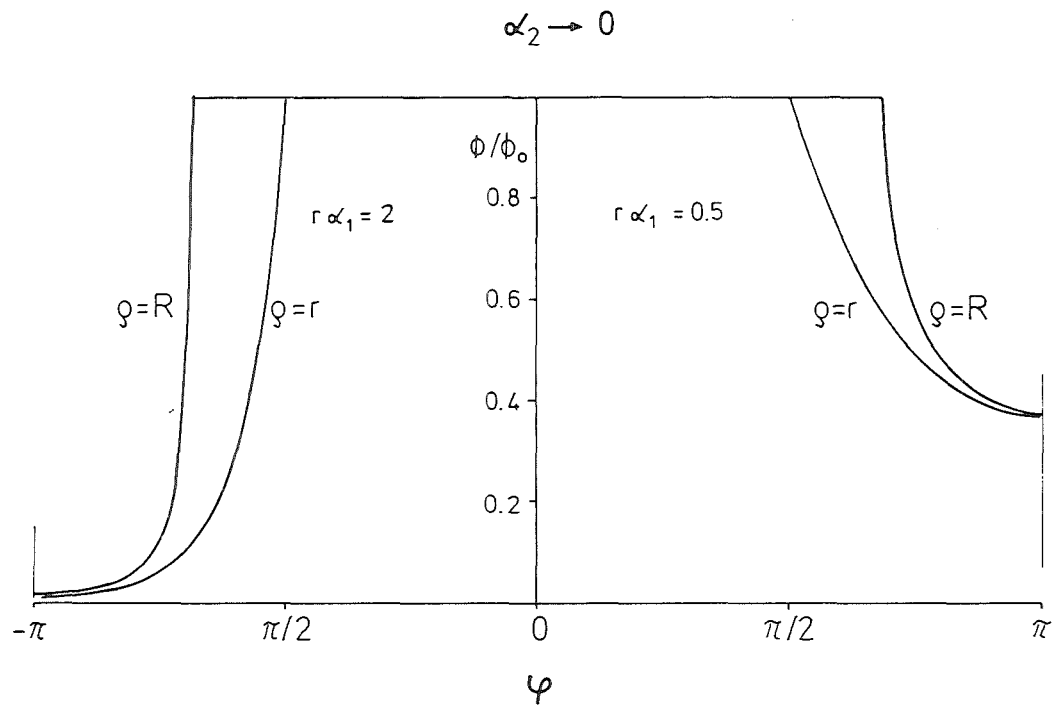
Figure 15   Distribution of neutron intensity in case of parallel
            neutron radiation
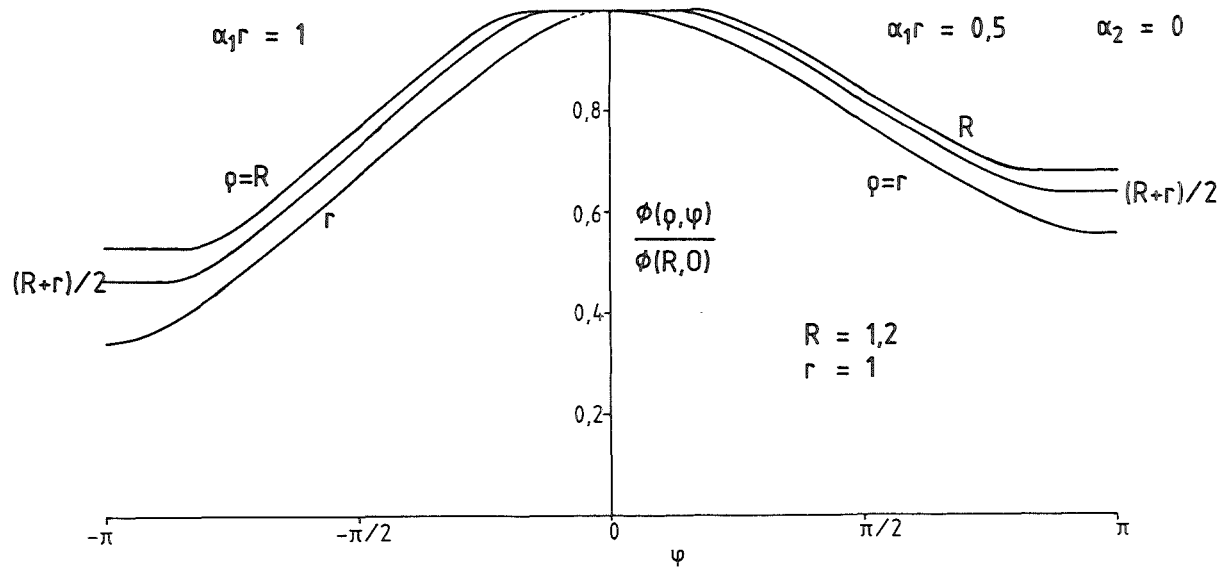
Figure 16   Distribution of neutron intensity in case of a tube in
front of a neutron radiating half-space
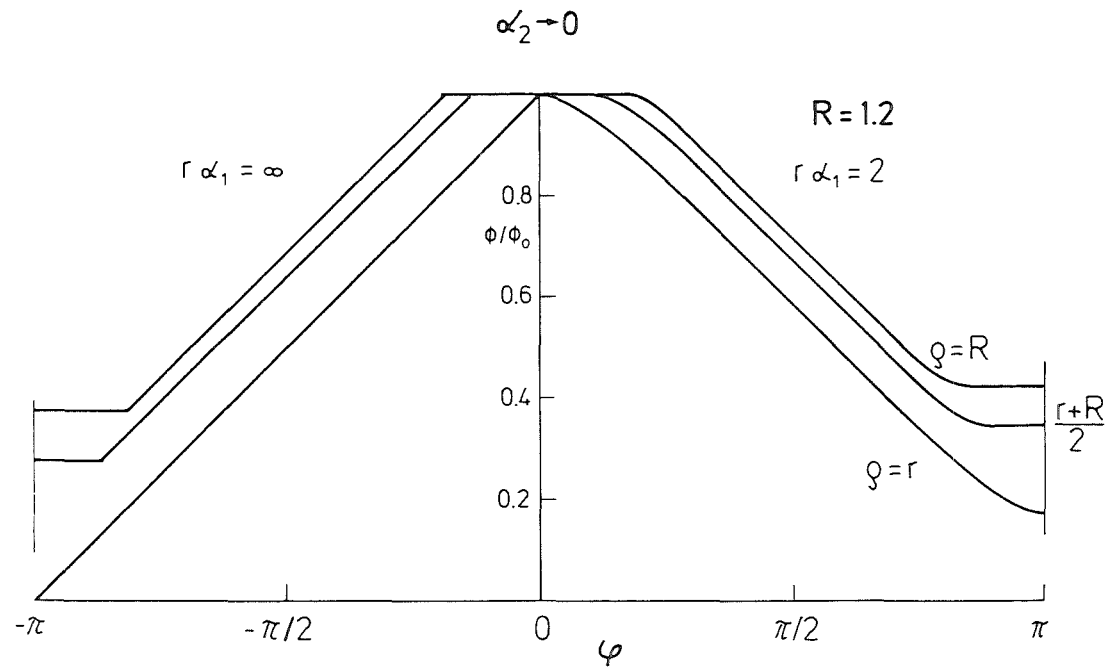
Figure 17 Distribution of neutron intensity in case of a tube in front of a neutron radiating half space
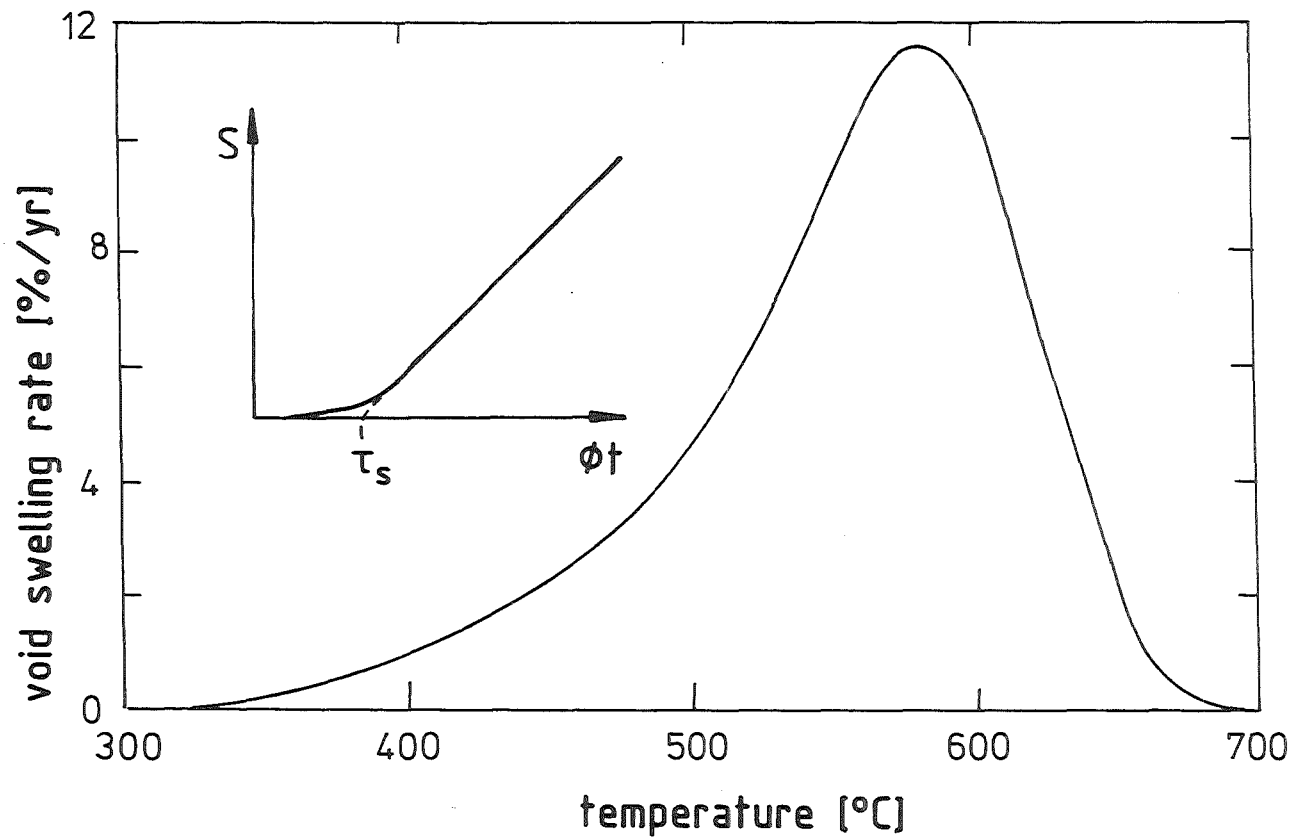
Figure 18   Void swelling rate for ϕ = 22 dpa/yr [6] (Insert:
time dependency of swelling, schematically)
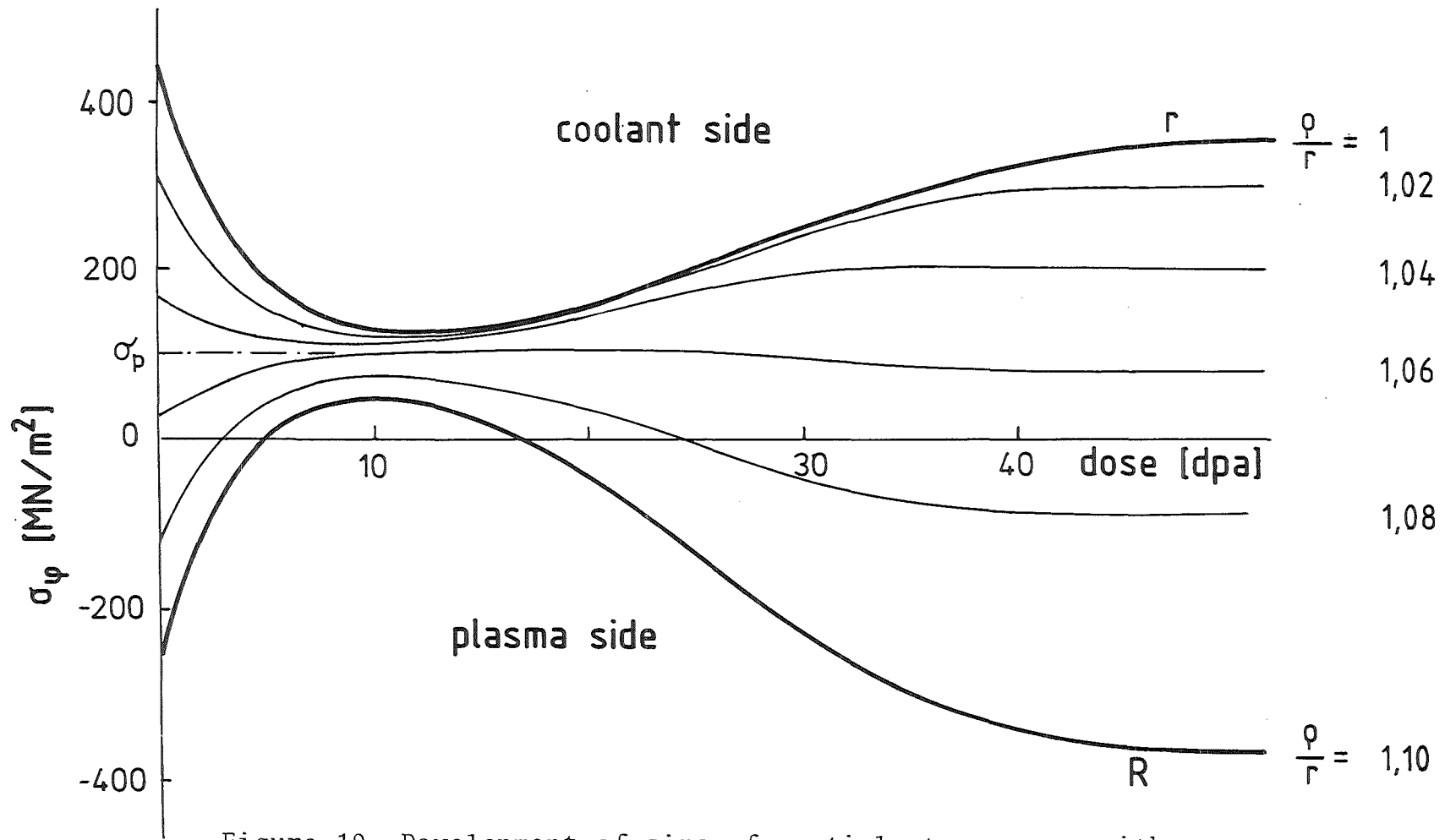
Figure 19   Development of circumferential stresses σ_φ with
increasing neutron dose
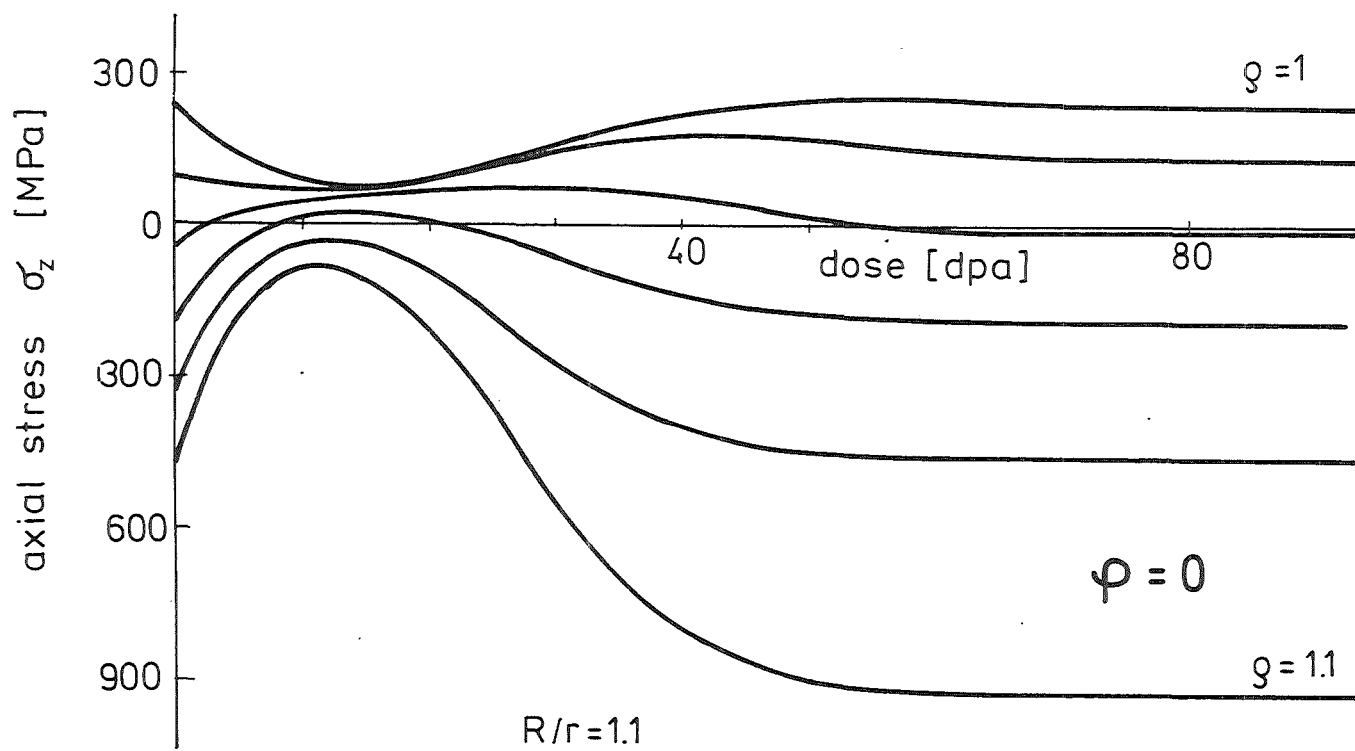
Figure 20   Axial stresses in the tube wall in dependence of
neutron dose
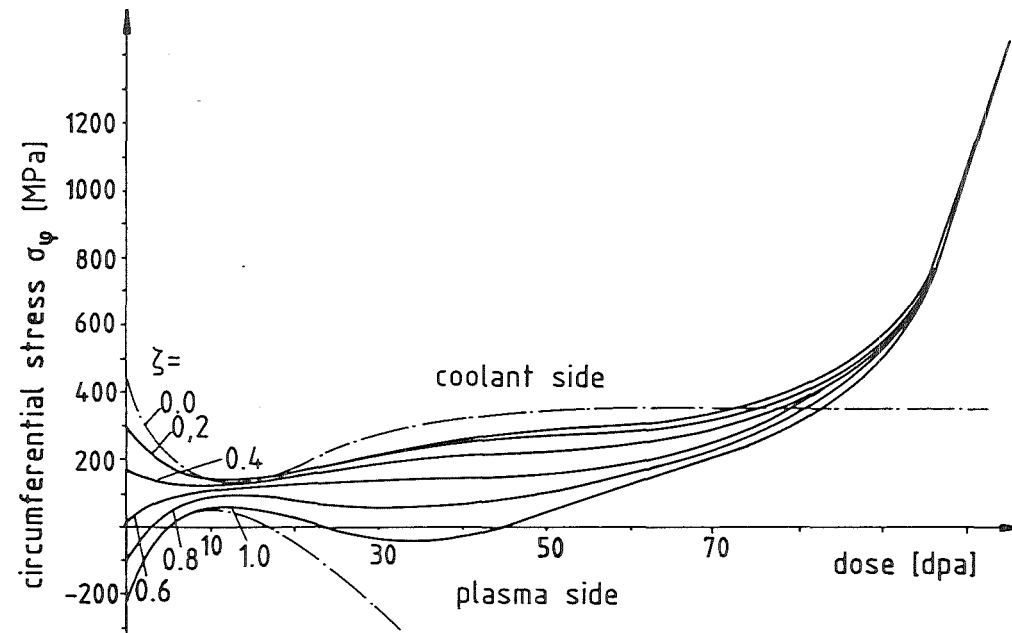
Figure 21   Influence of sputtering on circumferential stress σ
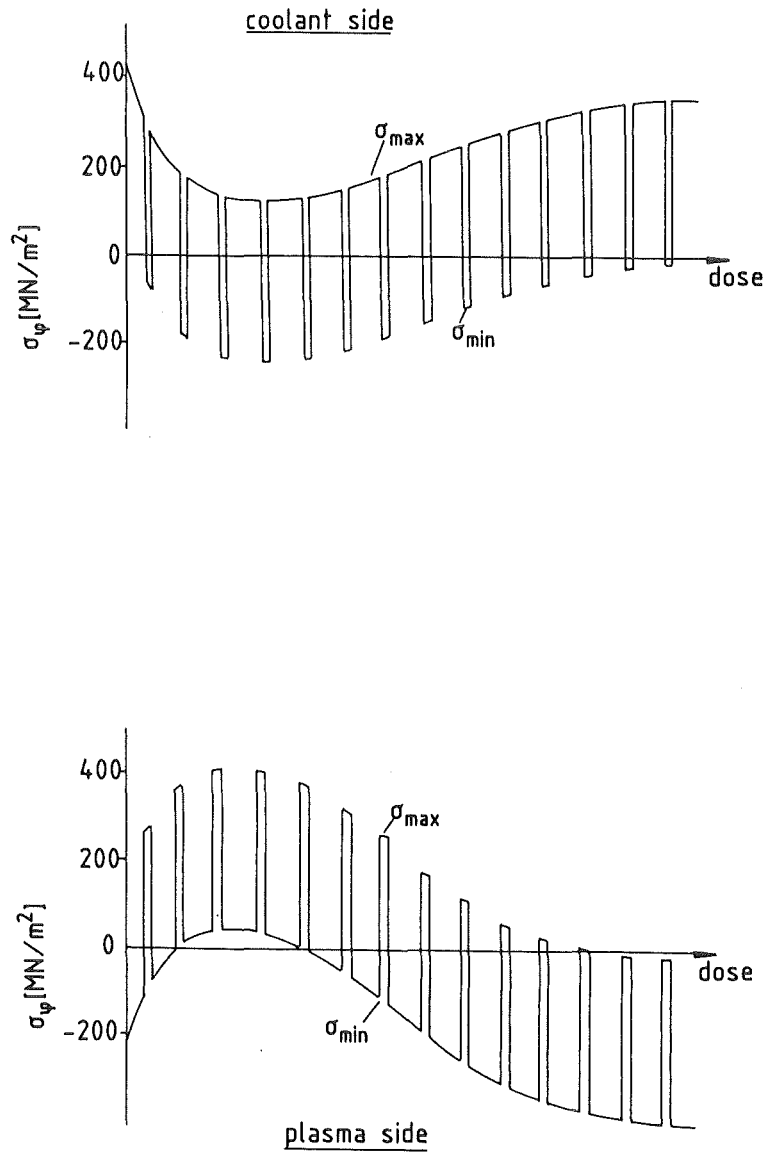
Figure 22   Circumferential stresses at the inner and outer side of a tube for cyclic operation
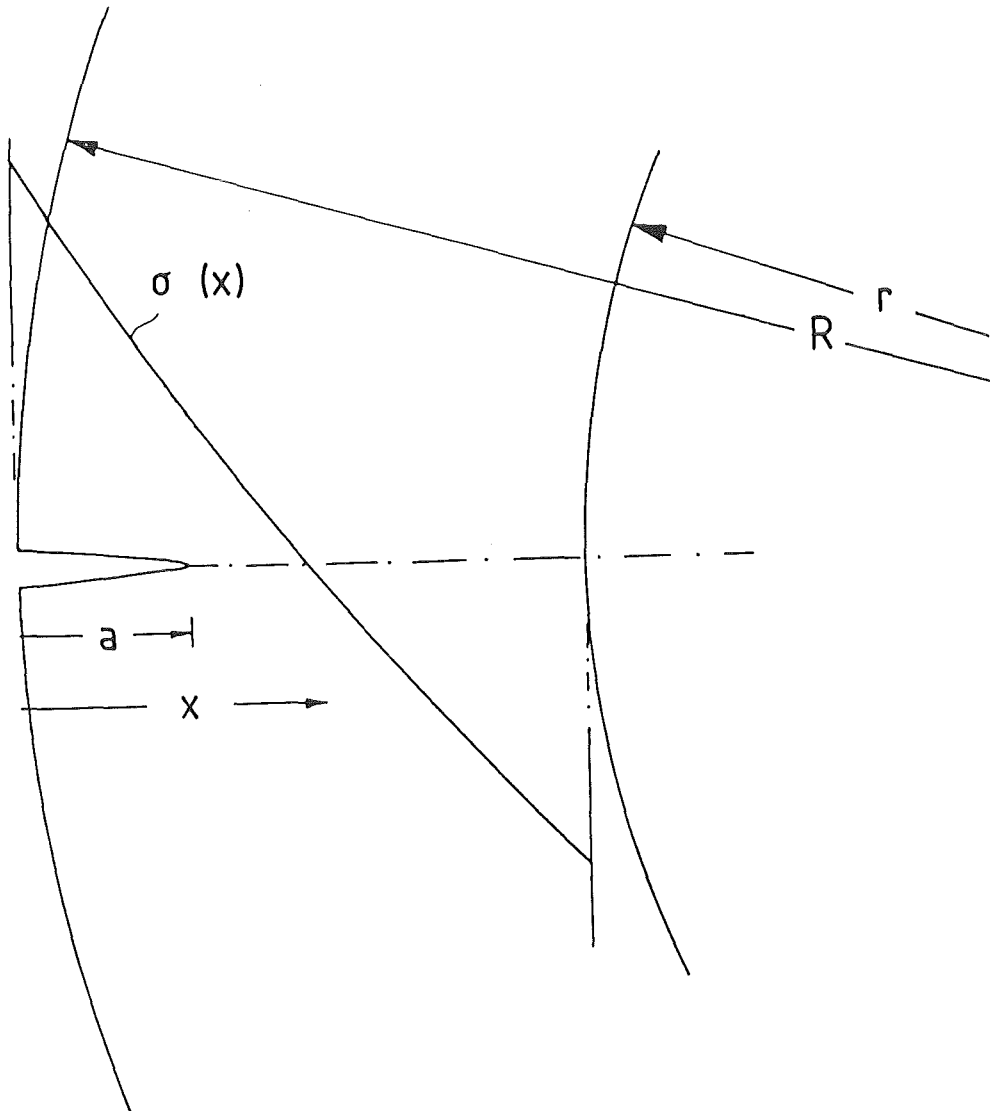
Figure 23   Crack in a tube wall affected by stress distribution
σ(x)
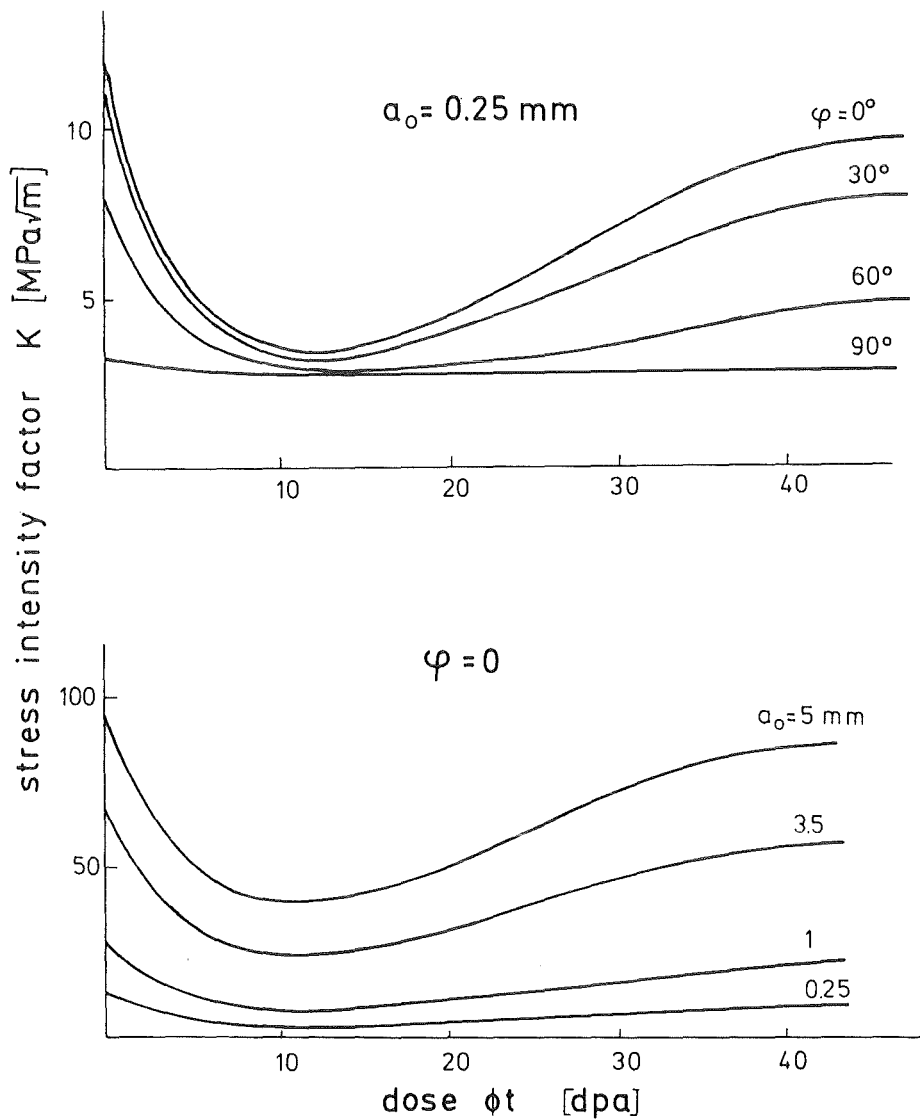
Figure 24   Stress intensity factors for inner surface cracks
(continuous operation)
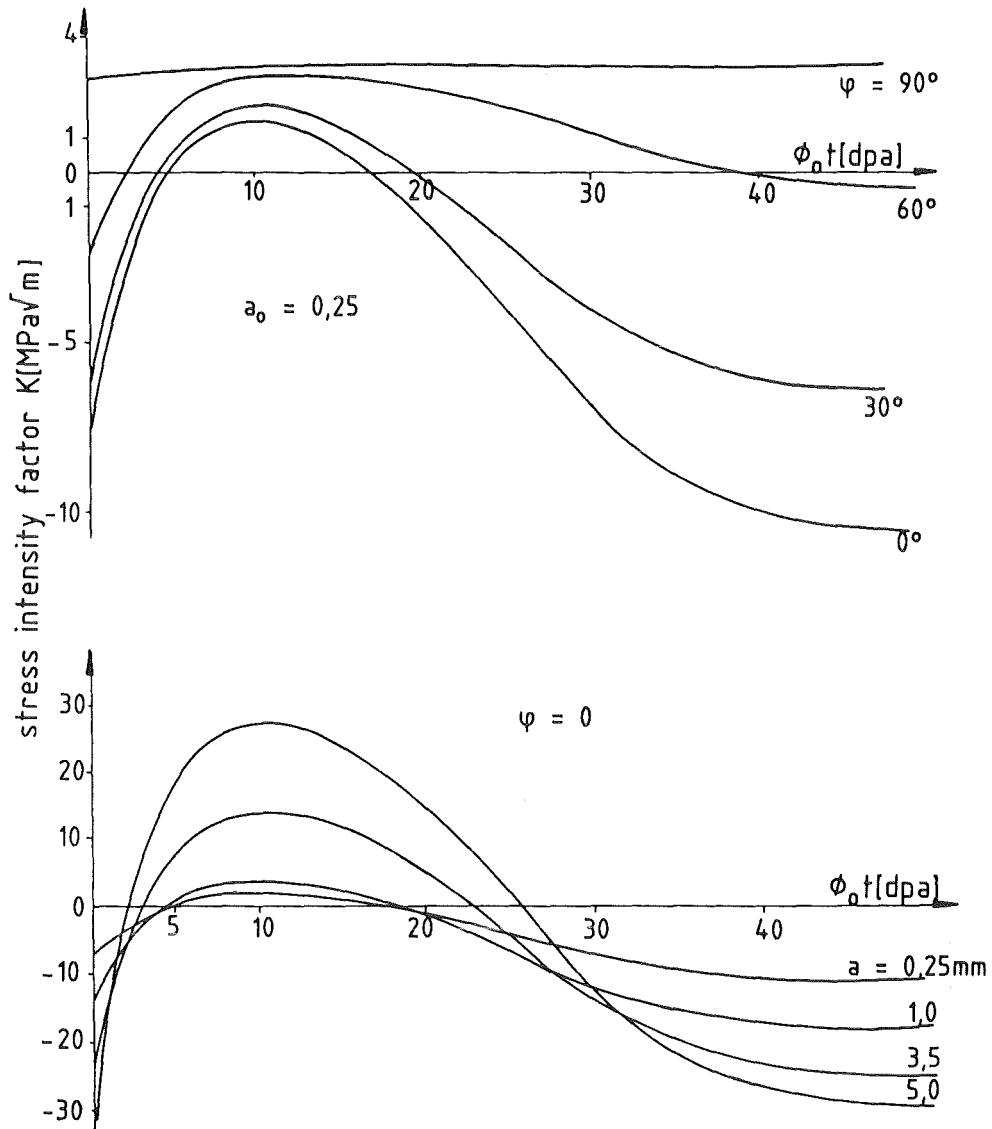
Figure 25   Stress intensity factors for outer surface cracks
(continuous operation)
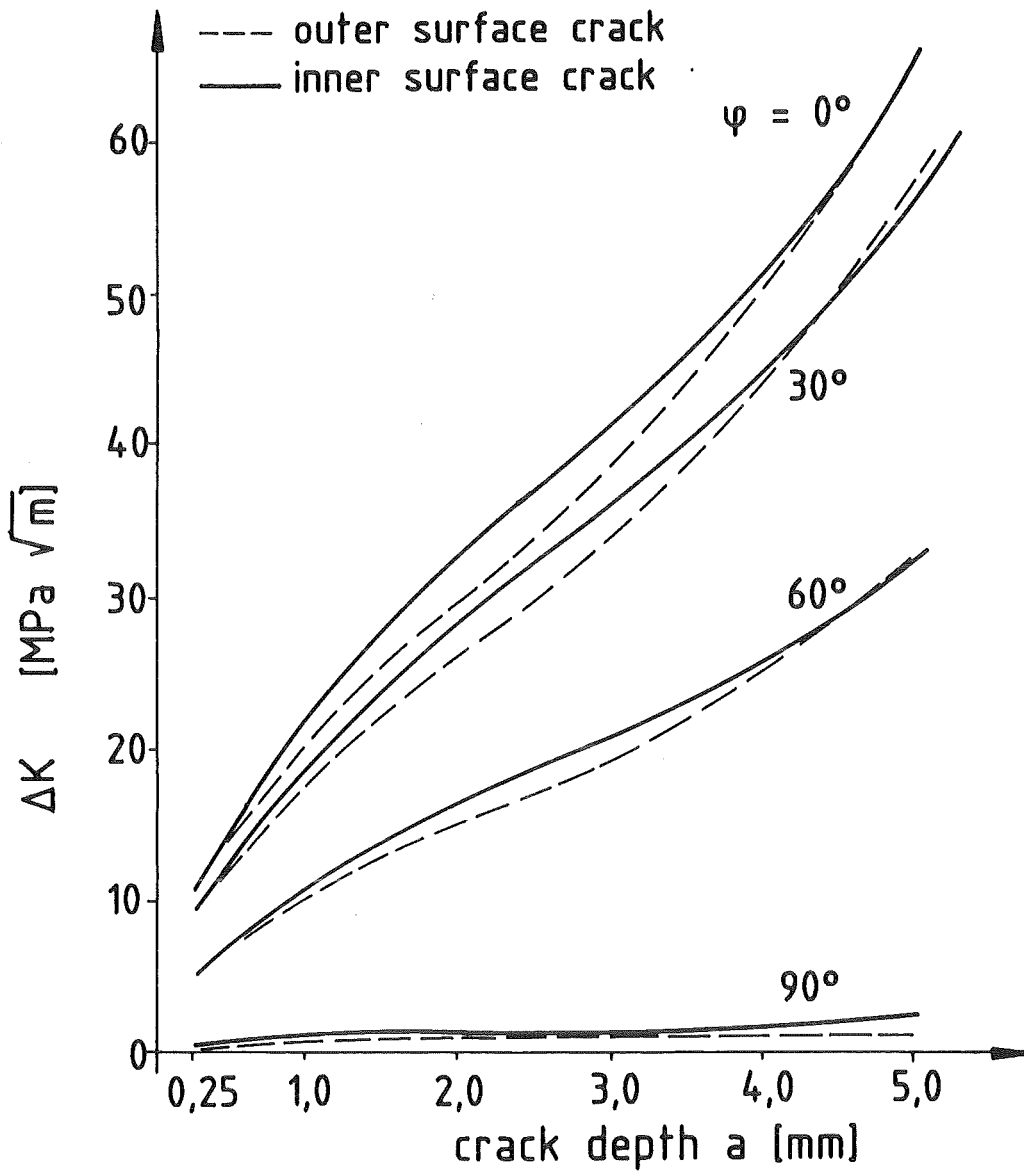
Figure 26   Cyclic stress intensity factors for inner and outer surface cracks
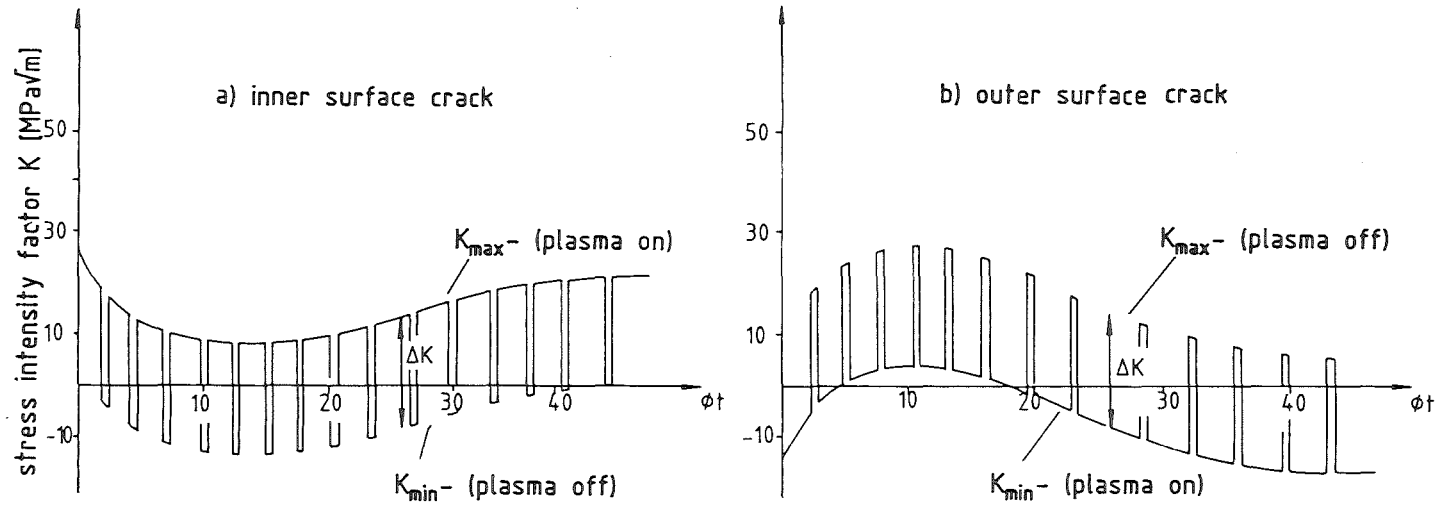
Figure 27   Stress intensity factor K for cyclic operation
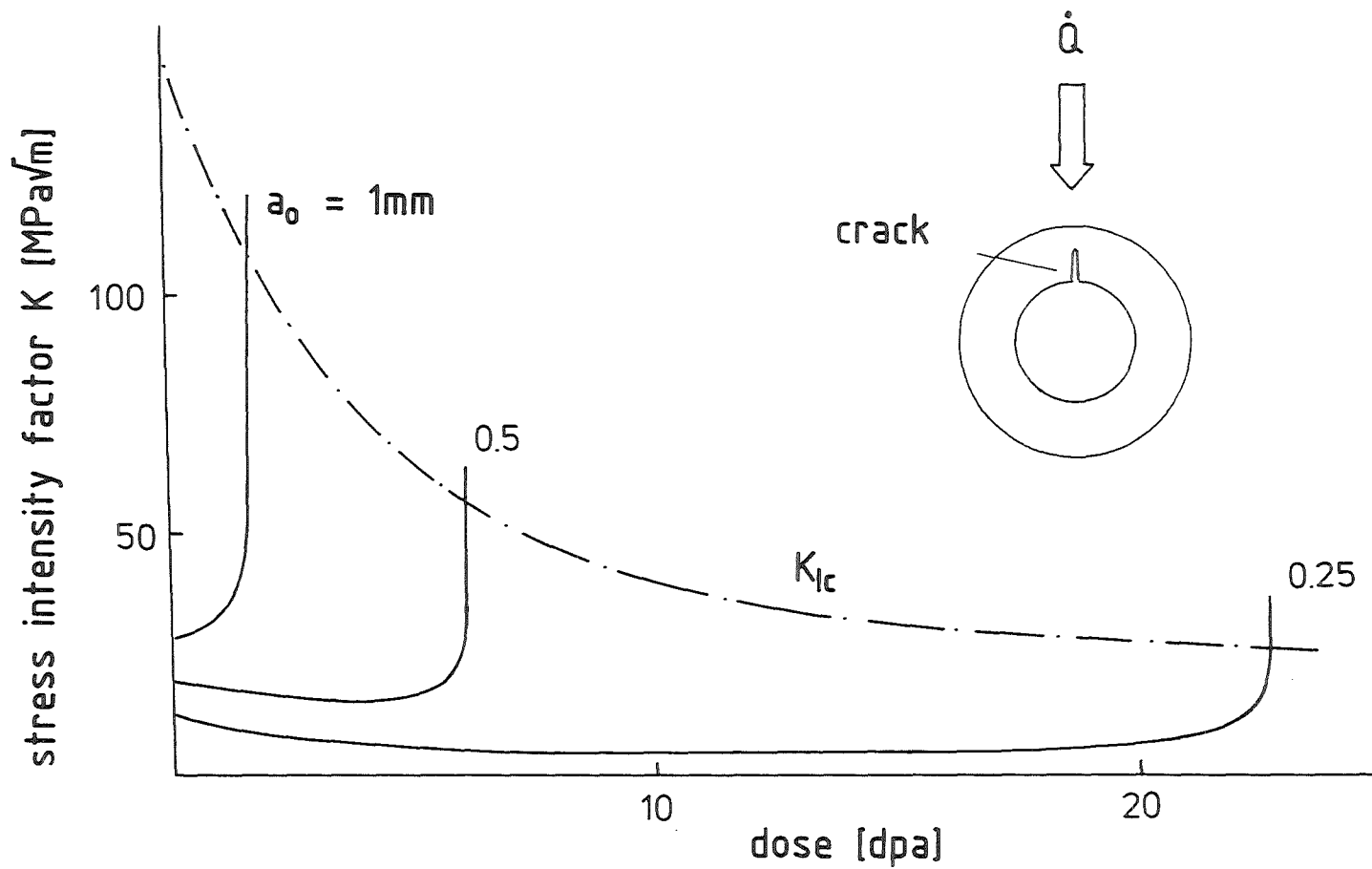
Figure 28   Fatigue crack growth and failure for inner surface cracks
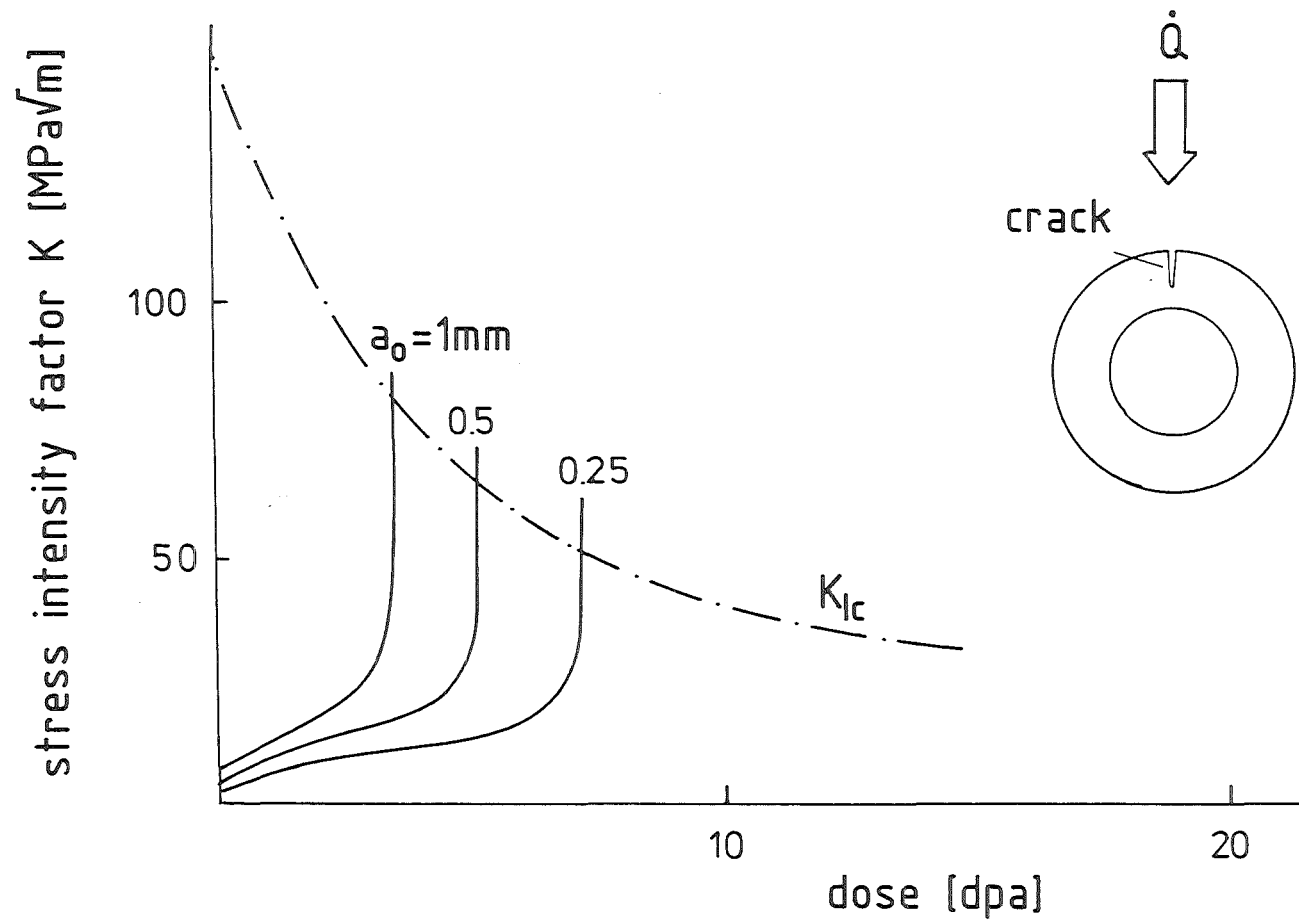
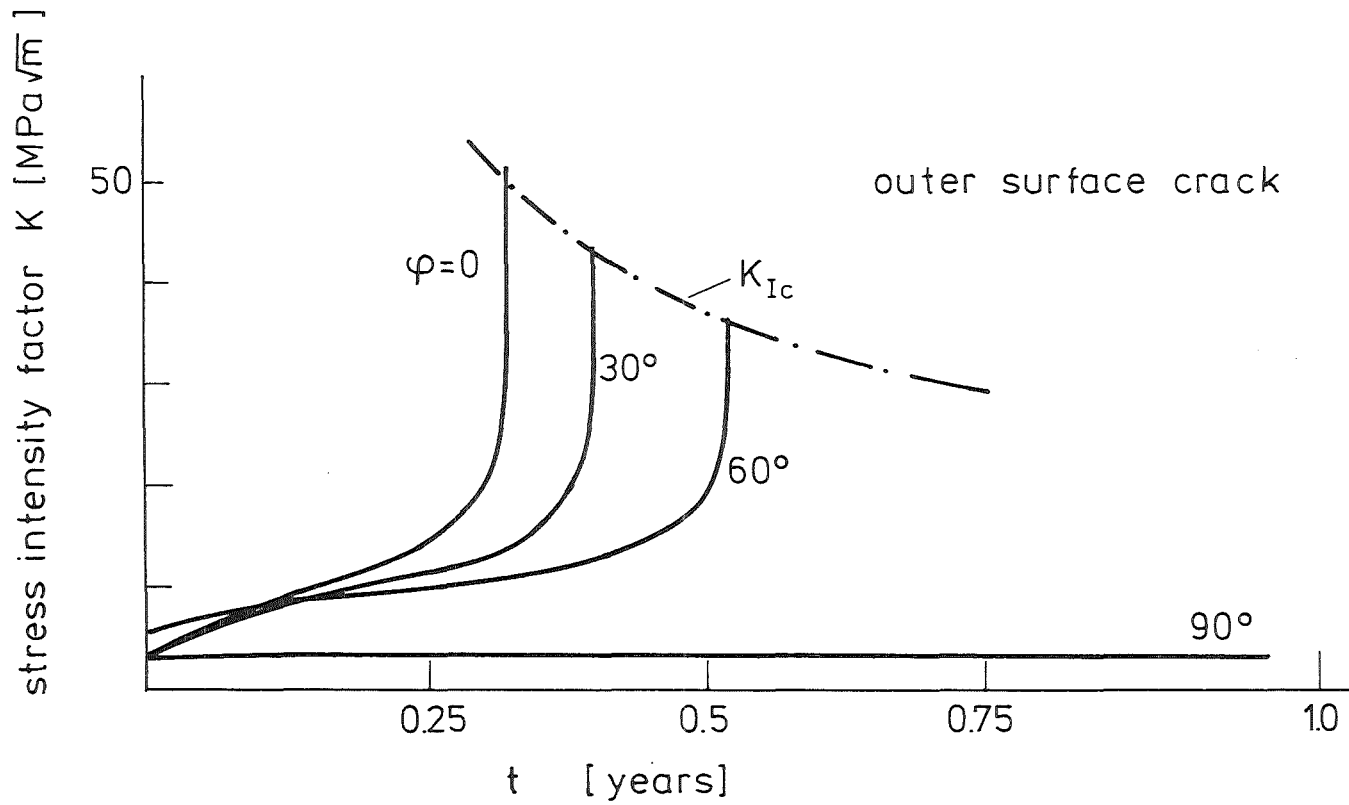Figure 29   Fatigue crack growth and failure for outer surface cracks

Figure 30 Fatigue behaviour in dependence of crack location for an outer surface crack with initial crack size $a_0 = 0.25$ mm
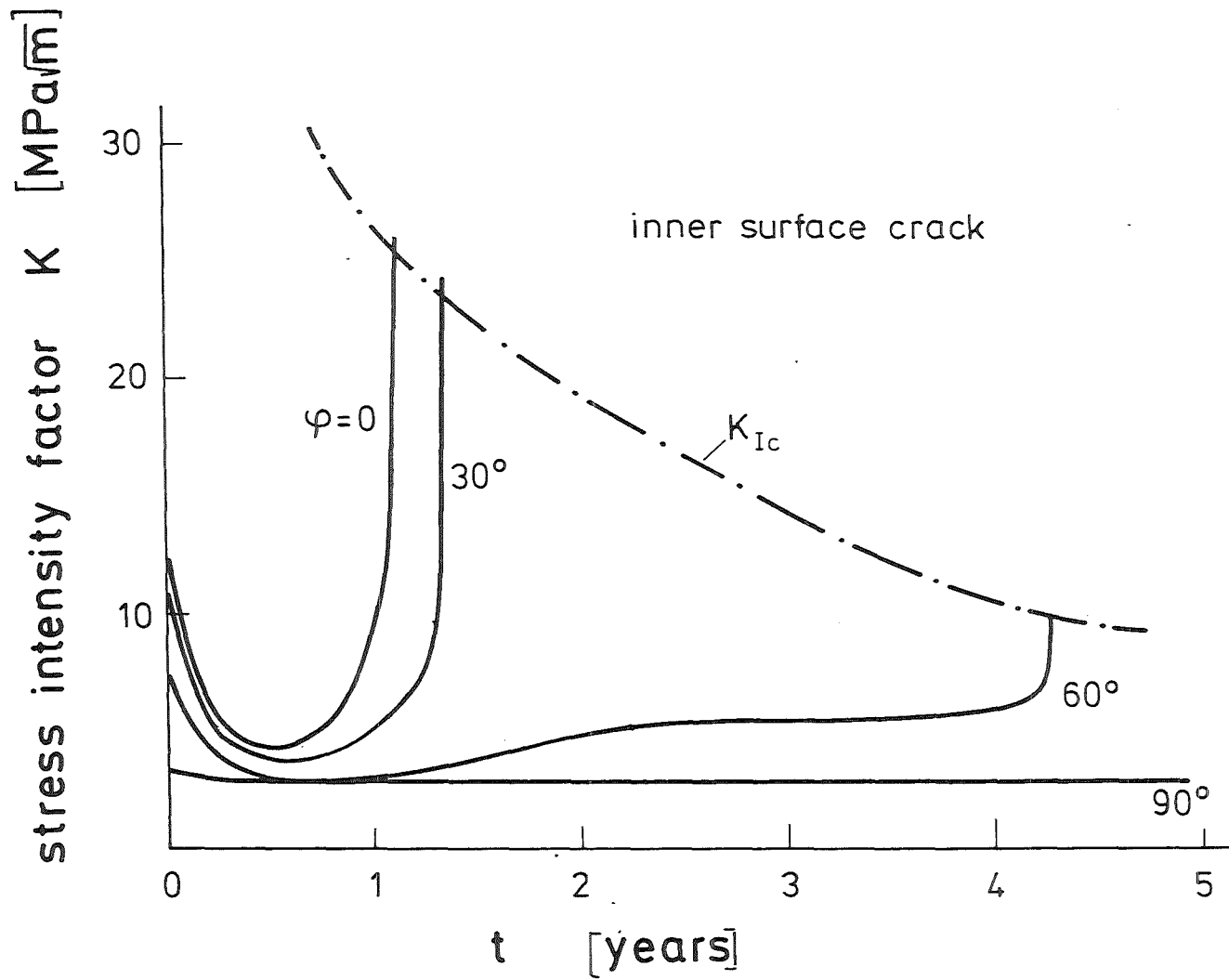
Figure 31   Fatigue behaviour in dependence of crack location for an
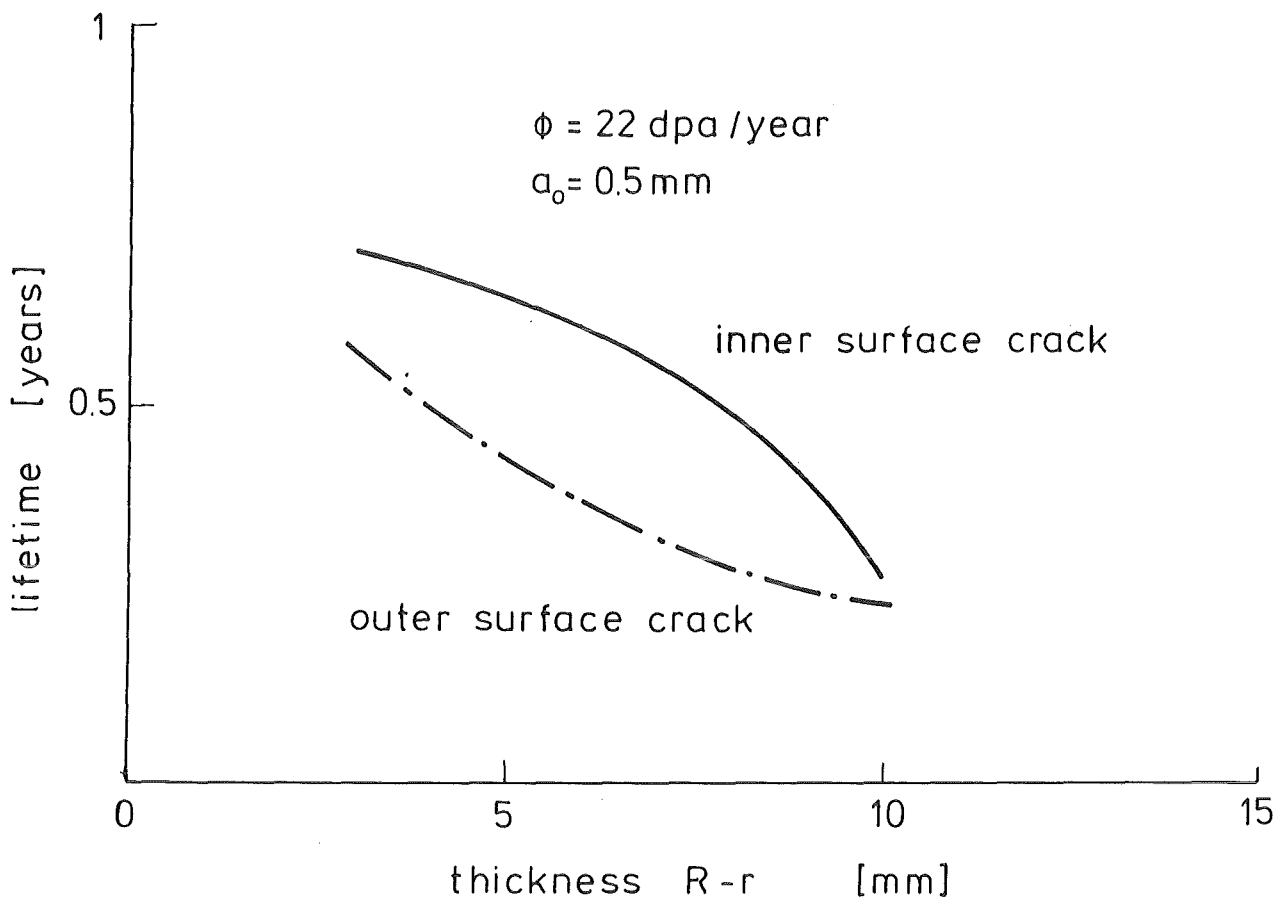inner surface crack with initial crack size a_o = 0.25 mm

Figure 32   Lifetime in dependence of tube wall thickness